MODELLING FOR CONTACT STRESS CONTROL IN AUTOMATED POLISHING

by

Avery Roswell

BEng in Mechanical Engineering, Ryerson University,

Toronto, Canada, 2002

A thesis

Presented to Ryerson University

In partial fulfillment of the requirement for the degree of

Master of Applied Science

in the program of

Mechanical Engineering

Toronto, Ontario, Canada, 2004

Declaration

I hereby declare that I am the sole author of this thesis.

I authorize Ryerson University to lend this thesis to other institutions or individuals for the purpose of scholarly research.

I further authorize Ryerson University to reproduce this thesis by photocopying or by other means, in total or in part, at the request of other institutions or individuals for the purpose of scholarly research..

Borrower's Page

Ryerson University requires the signatures of all persons using or photocopying this thesis. Please sign below, and give address and date.

NAME	ADDRESS	DATE

Abstract

Modelling for Contact Stress Control in Automated Polishing

MASc 2004, Avery Roswell, Mechanical Engineering, Ryerson University, Toronto

This research pertains to the initial steps in designing an end-effector for automated polishing, and focuses on: (1) controlling the contact stress on the work-piece surface, and (2) controlling the torque or the spindle speed to overcome the friction torque (hence, preventing the tool from stalling) and maintain a desired polishing rate. By forming a contact stress model, parameter planning is achieved and then augmented to already existing tool path data. A dynamic model of the particular end-of-arm tooling used is derived. The dynamic model clearly shows a coupling effect between the pressure and spindle speed of the system. A closed-loop control scheme, designed to eliminate the coupling is then introduced. The effectiveness of parameter planning is assessed through open loop testing. The parameter planning method allows polishing without significantly changing the part profile, whereas, without the parameter planning, the part profile is changed considerably.

Keywords: Active compliance control, automated polishing, contact modelling

Acknowledgements

I would like to express my gratitude to Prof. F. Xi for his constant guidance and enthusiasm during this research thesis. His patience and understanding were profound and very much appreciated. Many thanks to Prof. G. Liu, my co-supervisor, although this thesis research is far from being control theory intensive, his shared insight and professionalism was exemplary. For the use of his laboratory and the Cobra-2D Laser Profile Scanner, I thank Prof. Ghasempoor, and his student Yi Yang. Steven Yang and John Sun are also fellow students, and I appreciate their collaborative effort.

Many thanks to Devin Ostrom, a Technical Officer of the department of Mechanical, Aerospace and Industrial Engineering – for his outstanding technical support. For the administrative aspect, Leah Stanwyck , the Graduate Studies Program Assistant for Mechanical Engineering, has been a blessing, always willing to help and never without a warm smile – many thanks to her.

Personally, I thank my God and His servant and child, Norma Kwarten. This has been an experience never to be forgotten. In thanking Him, I thank all those persons He has allowed to be in my life. Hallelujah.

Table of Contents

List of Figures

List of Tables

Nomenclature

A	contact surface area
A_c	cross-sectional area of the pneumatic cylinders
A_x	cross-sectional area inlet port of the polishing tool
a	semi-major axis of an ellipse
b	semi-minor axis of an ellipse
c	represents maximum or principal contact stress
$\mathrm{c_p}$	specific heat capacity at constant pressure
$\mathrm{c_v}$	specific heat capacity at constant volume
d_t	tool's diameter
$d(.)$	infinitesimal quantity
e	angle between x-axis and segment
e	exponential function
$\mathrm{e_1}$	the tracking error
E_1	Young's modulus of elasticity for polishing tool
E_2	Young's modulus of elasticity for the work-piece
$E(.)$	complete elliptic integral of the second kind
F	force
F_c	force exerted by pneumatic cylinders
F_f	kinetic friction force; damping
F_s	the reaction force between the polishing tool and the work-piece
F_{sf}	friction force between the polishing tool and the work-piece
$\mathrm{G_p}$	the transfer function pertaining to the electro-pneumatic valve
$\mathrm{G_q}$	the transfer function pertaining to the flow valve
H_f	transfer function for force sensor
H_p	transfer function for pressure sensor
H_w	transfer function for rotational speed sensor
I	the moment of inertia of the polishing tool head
k	ratio of semi-minor to semi-major axis
k_s	spring stiffness
$K(.)$	complete elliptic integral of the first kind
M	mass of the polishing assembly

m	the mass of air in the pneumatic cylinder chamber
P_c	pressure in pneumatic cylinders
ΔP_c	change in cylinder pressure
P_{in}	power input to the polishing tool
P_m	mean contact stress or average contact stress
P_o	maximum contact stress
P_{out}	power output from the polishing tool
P_s	pressure or stress across the non-hertzian contact surface
P_{seg}	pressure or contact stress at a particular segment on the contact surface
p_s	the supply pressure
p_x	the exhaust pressure
$Q(z)$	curvature as a function of the work-piece height, z
q	volumetric flow rate
R	maximum radius of the contact surface
R_1	minimum radius of curvature of the polishing tool
R'_1	maximum radius of curvature of the polishing tool
R_2	minimum radius of curvature of work-piece
R'_2	maximum radius of curvature of work-piece
R_f	the resistance of the fluid flow within the pneumatic spindle
r	radius of contact surface
T_R	the resultant torque
T_c	temperature of the air in the cylinders
T_f	friction torque
T_p	applied polishing torque
t	time
V	velocity
V_c	the volume of the cylinder chambers
ΔV_c	change in cylinder volume
$\mathrm{V_p}$	voltage input variable for the electro-pneumatic valve
$\mathrm{V_q}$	voltage input variable for the flow valve
x	Cartesian x-axis coordinate
y	Cartesian y-axis coordinate
Z	distance or depth from the contact surface area; this depth being along the z-axis

z	represents the variation of stress at different x and y values; also the displacement along z-axis
$\ddot{z}$	acceleration in the z-axis direction

Greek Symbols

γ	the ratio of specific heat capacity at constant pressure to specific heat capacity at constant volume
η	mechanical efficiency
π	pi
ρ	the density of air in the cylinder
μ_k	the coefficient of kinetic friction
σ_{zz}	principal stress on the contact surface
ν_1	Poisson's ratios for the polishing head
ν_2	Poisson's ratios for the work-piece
ϕ	the angle between the corresponding planes of the principal curvature (i.e. between R'_1 and R'_2, or between R_1 and R_2)
ω	angular or rotational speed
$\dot{\omega}$	angular or rotational acceleration

CHAPTER 1: Introduction

This chapter provides a background on metal die polishing, as well as the resources and considerations necessary to automate the polishing process. Subsequently, the problem-statement and scope of the thesis are given. Finally is the thesis outline, which supplies the reader with a description of the organizational layout of the thesis material.

1.1 Background

In the manufacturing industry, polishing of moulds and dies consumes gross amounts of resources and time. The purpose of polishing is to reduce the surface roughness to a desired level. Generally, the polishing process first involves removing scratches, machining marks, pits, and other defects before finally obtaining the desired surface finish [1]. According to Guvenc and Srinivasan [2], approximately 37% of manufacturing time is allocated to finishing the mould cavity's surface. This large percentage of time is indicative of the complexity of the tool motions necessary, the wide variety of tooling utilized, as well as measuring and recording the surface quality during the process. As one can imagine, this expensive and time consuming polishing process relies heavily on skilled labour.

Accordingly, automated polishing would be invaluable in the industry and the cost savings would be substantial. This fact has attracted extensive research to investigate possible methods of designing and implementing automated polishing systems [3-7]; these systems involve force control or regulation. The Intelligent Manufacturing Systems (IMS) has also taken the initiative of forming a Community of Common Interest (CCI) in Die and Mould Design and Manufacturing (DMDM-CCI) [8]. IMS is an industry-led, collaborative, international research and development network established at the inter-government level; its goal is to further manufacturing and processing technology. So far, the DMDM-CCI is comprised of representatives from small, medium and large companies, research institutes and academia from Canada, Australia, the EU, Japan, Korea, Switzerland and the U.S.A. [8]. This highlights the international interest in the area of die and mould manufacturing. The British company, Broadbans Engineering, quickly cut their mould manufacturing lead times by implementing automated EDM (electro-discharge machine) centres [9]. Additionally, Glen Carlson, Chairman of Acme Manufacturing Co. in Michigan, wrote an article outlining advances in automated polishing, buffing and deburring [10]. He claims that both small and large manufacturing plants must continue to upgrade their finishing operations and facilities. Companies need to meet future manufacturing goals and hence manual finishing methods have become less desirable and even ineffective in some instances. Besides this, labour shortages of qualified and trained personnel continue to affect most of the United States manufacturers. People are not keen on working in polishing and deburring environments. With automated machines, such as robots, computer-numerical control (CNC), programmable-logic control (PLC), and PC-based devices critical market factors may be addressed. These critical factors are: (1) machine flexibility, (2) improved part quality and consistency of finish, (3) reduced finishing costs and better utilization of abrasive media, (4) operator safety and environmental regulations, (5) improved part handling and scheduling procedures to minimize inventory and in-process manufacturing costs, and (6) the growing shortage of trained and qualified or willing labour [10].

1.1.1 Conceptual Framework of Automated Polishing

Various advanced automated systems with application to polishing, grinding, and deburring have been proposed over the years, all inherently consisting of a basic core structure. This core structure is comprised of a process planner, a control system, and a plant (i.e., the physical structure and environment being controlled). Additional components include computer-aided-design (CAD) systems, computer-aided-manufacturing (CAM) systems, and measurement systems feeding back to the process planner.

Considering the advance deburring paradigm proposed by Murphy and Proctor [11], and the conceptual automation structure by Guvenc and Srinivasan [2], the following steps are necessary for automated polishing:

1. A comprehensive description of the part to be polished must be developed.
2. The process planner then associates the tool and tool parameters with the particular geometry of the part.
3. The controller performs trajectory planning and computes the sequence of the robot's required path. (The controller may also encompass tool force adjustments if active control is being applied.)
4. The controller interfaces with the polishing process (i.e. the plant) and this is where dynamic interaction with the real world occurs.

The below diagram, Figure 1.1, gives an example of a basic core, with the addition of surface measurement.

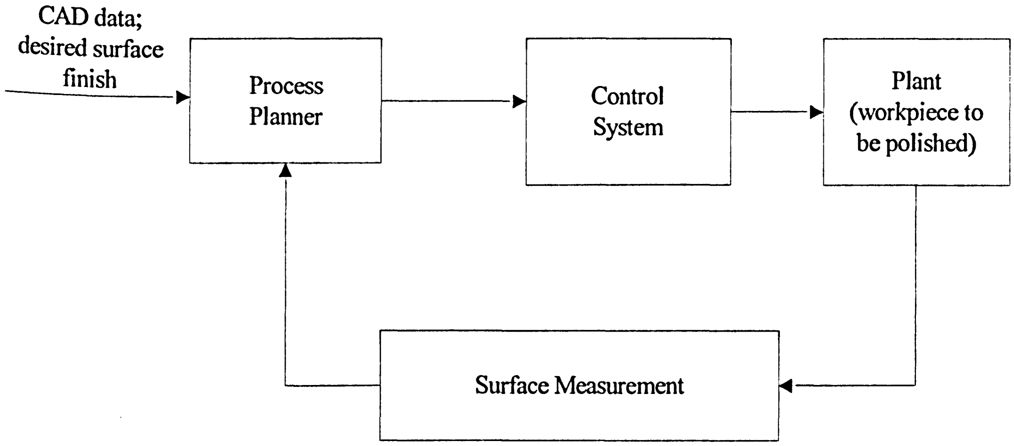

Figure 1.1 Block diagram of Conceptual structure of an automated polishing system

Emphasis will be solely placed on the sub-systems within this conceptual framework (illustrated above) that pertain to dynamic model-base control, and they are, consequently, the control system and its interaction with the plant system. Not only does one focus on this interaction, but also the interaction within the plant – between the polishing tool and the part being polished. This brings attention to the tool-fixture design philosophy.

1.1.2 Tool Fixture Design

In most automated finishing processes, the machine performing the process holds the tool (in this instance a polishing tool), whether the machine is an industrial robot arm or a CNC machine, or some combination of the two. A tool device is therefore required to attach the particular polishing tool to the machine. The particular design of the tool holding device mainly depends on the interaction between the polishing tool and the part (work-piece), and the type of force control technique employed to perform the process (e.g. through-the-arm, active, or passive control; these will be explained in the following paragraphs).

For a further break down, the Figure 1.2 below illustrates the sub-systems contained within the main control and plant system blocks of Figure 1.1, as well as their interaction.

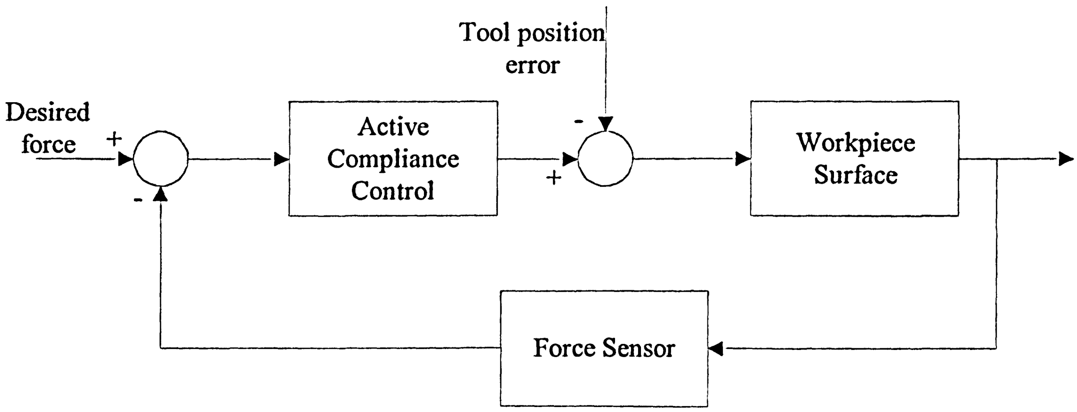

Figure 1.2 Illustrating sub-systems of the conceptual automation framework

When performing polishing with a non-compliant polishing head (i.e., the polishing head is not flexible; it cannot change shape to fit the geometry of the work-piece), the compliance is only due to a passive or active control system. Types of control techniques and systems are discussed in the sections to follow, but to give the reader an understanding of the present discussion, a brief description is provided. Passive or active compliance is the ability of the tooling device to compensate in particular axes when there is a position or force error during the automated process. Active compliance requires at least one actuator to perform the compensation, while passive compliance may be achieved via a mechanism of links and springs, for example.

Similar to deburring, for polishing the normal direction of an actively controlled tool fixture must be compliant allowing the polishing head to remain in contact with the work piece surface during the polishing process. Loss of surface contact between the tool and the work piece is due to position errors. In addition, the force applied to the work-piece from the polishing tool head must be maintained within a specified range and in some cases an exact value, and so this goes beyond the simple matter of keeping the polishing head and work-piece in constant contact with each other. Figure 3 illustrates the compliance arrangement applied during deburring processes and it is assumed that a similar model is appropriate for polishing.

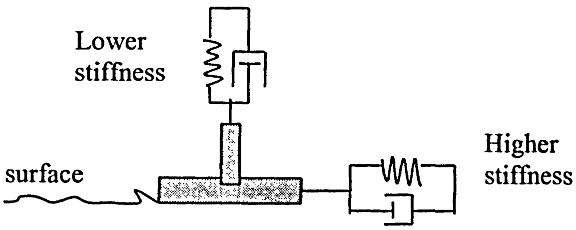

Figure 1.3 Tool fixture dynamics

The normal direction would have less stiffness than the tangential direction. This allows for the much-needed normal compliance, which can accommodate various fluctuations of the polishing force, while still applying a firm force in the tangential direction. The researchers, Guvenc and Srinivasan, have justified this model after conducting polishing experiments.

Along with the stiffness criteria mentioned above, the end-effector also requires three important capabilities or functions, which are listed below:

1. Measure the orthogonal (normal) contact force between the polishing head and the work-piece.

2. Measure the polishing head's position and orientation relative to the work piece surface, in particular, angular misalignments.
3. Real-time control of the orthogonal force applied by the polishing head, as well as, the control of the angular alignment – with the objective of keeping the polishing head parallel to the work piece surface.

These three capabilities are similar to those given by Engel et al. [12] in their research: "Concept for Robotic Deburring Using Multipass Active Control". The given capabilities two (2) and three (3) are different from their work by considering angular misalignment relative to the work piece surface, as well as methods of correcting such misalignment.

Barratt et al. address tool-to-part misalignment in their research on "Automated Polishing of an Unknown Three-dimensional Surface" [13]. This misalignment refers to the tool not being normal to the work-piece. Using a passive compliant end-effector mounted on the wrist of an industrial robot, they were able to maintain contact with the work surface within an angular range of $\pm$ 8 degrees and a $\pm$10 mm range of normal (orthogonal) translation movement. In their experiment, the researchers relied solely on contact geometry to correct the trajectory of the robot.

In this body of research, the first (1) and third (3) capabilities are investigated, i.e. the measurement of the applied force and its control in the direction normal to the work-piece surface.

1.2 Problem Statement

The objective of force control based polishing processes has been to maintain a constant applied force on the polishing tool, resulting in a uniformly polished part. This assumes the polishing speed or velocity remains constant throughout as well. For a rotating polishing tool, this means a constant feed-rate and spindle speed.

However, this constant polishing force does not guarantee a constant contact stress between the polishing tool and the part being polished when the part's surface geometry changes significantly. Under this circumstance, the contact stress determines the quality of the polished part, and not the force exerted on the polishing tool. With a constant force applied to the polishing tool, the contact stress will change from point to point as the part geometry varies, leading to variations in the torque and speed of the polishing tool.

If the contact stress is too high, the part will be over polished (i.e., a change in profile); if the polishing tool's speed varies the polishing will be non-uniform; and so this is the presented problem – **to maintain a constant surface contact stress and spindle speed during automated polishing.**

Maintaining or regulating stress and speed entails a control system. From point to point along the tool trajectory, a control system must adjust the applied polishing force and spindle speed to produce the desired surface contact stress and spindle speed. Essentially this is force tracking and so the problem extends to applied polishing force planning, as well as providing a particular polishing spindle speed.

1.3 Scope

This thesis research documents the initial steps in designing an end-effector or end of arm tool (EOAT) to be used for automated metal die polishing. The particular EOAT is to facilitate the control of the contact stress on the metal work-piece during polishing, and give the necessary compliance for such a finishing process as polishing.

An approach for maintaining a constant surface contact stress has never been attempted before, and as this is the initial approach, the EOAT is limited to polishing free-form metal surfaces (having a large radius of curvature). A surface whose shape is not constrained by classical analytical forms (such as conic surfaces) and which is defined by a set of control points (as with Bézier, b-spline, and NURBS surfaces) is known as a free-form surface.

Performing parameter planning pertains primarily to the applied polishing force. As for the rotational polishing speed (spindle speed), it is only necessary to regulate the rotational speed, maintaining the specified revolutions per minute. The applied polishing force parameter augments the already existing path planning data. Note that in this particular research, because pneumatic cylinders are used to generate the polishing force, the cylinder pressure may replace force in the parameter planning process.

This thesis also proposes a dynamic model with a corresponding control system to achieve the necessary tracking of the generated parameter, as well as regulating the rotational speed.

1.4 Thesis Outline

There are seven chapters ahead. Chapter 2 provides a Literature Review of the existing machines in industry, control methods employed to achieve automated finishing processes such as grinding and polishing, contact modelling (i.e. interaction between the tool and work-piece), and the currently used path planning methods. Chapter 3 deals with the occurring contact stress between the polishing tool and part, during the polishing process, while chapter 4 goes a step further by analyzing the friction torque arising between the spinning tool head and the part's surface.

After the discussion of contact stress and friction torque (as well as spindle speed), the parameter planning of applied force (through the actuation of pneumatic cylinders) and spindle speed is explained and demonstrated in chapter 5. Chapter 6 then introduces the existing system's dynamics, that is, the system used to perform the experiments. With a dynamic model complete, an appropriate control scheme is proposed. Following are the experiments performed, and the procedure and results documented in chapter 7.

The final chapter (chapter 8) is a discussion and conclusion of this research. After the chapters come the appendix and references, respectively.

CHAPTER 2: Literature Review

Before confronting the challenges undoubtedly present in the endeavour of contact stress control for automated polishing, existing efforts, both past and current, should be examined. The machines, control methods, contact modelling, and tool-path generation (i.e., path planning) are important factors. They are reviewed in this chapter, drawing from engineering textbooks, research journals, and industry articles.

2.1 Machines

Previous and current approaches to automate mould polishing can be loosely classified based on whether a conventional machine tool structure (e.g., computer-numerical control – CNC) or an articulated robot arm (i.e. industrial robots) is being used [11]. Within each classification, the force control methods employed can also be broadly categorized as through-the-arm end-effector force control and active (or passive) end-effector force control [11].

Computer-numerical control (CNC) machines are attractive and have been adopted in the past due to their high stiffness and accuracy. However, CNC machines are expensive and have a limited number of axis and range of motion; this restriction on motion confines the CNC machine to particular applications only. The articulated robot arm has greater axis of motion, allowing them to possess larger work volumes at less cost than CNC machines; this comes, consequently, at the loss of stiffness and accuracy. A compromise must be met between the limited motion of the CNC machine and the lack of accuracy and stiffness of the robotic based polishing, for success. In fact, the combination of a machining centre with an industrial robot does exist, and the researchers, Lee et al. [14], used a three-axis machining centre and a two-axis polishing robot to successfully perform automated polishing. Aside from this, various methods of force control have been employed to compensate for robots inaccuracies and lack of stiffness, in their use for finishing (i.e., grinding, deburring, and polishing), and are presented below.

2.2 Through-the-arm Force Control

Through-the-arm force control is a well-known technique where force sensory feedback is used to determine the tool-to-part contact, and the machine's position is adjusted accordingly. The machine moves all its axes simultaneously to obtain the required end-effector force and motion. One can immediately notice the combination of position and force control. This combination is referred to as hybrid control (or hybrid position/force control) [15-17].

In through-the-arm control, not only is there low force resolution due to joint friction, but there are large time lags associated with robot joint servo responses and large dead times due to one controller performing both force and position control. These deficiencies are usually indicated by the robot bandwidth, which is a measure of the overall robot system response. Robot bandwidth is constrained by the robot controller's computational speed, the communication protocol between the host computer and the servo hardware, and physical quantities such as inertia, motor response, and joint friction [11]. A low bandwidth, which equates to a slow response, prevents the robot from reacting to high-frequency control signals required in the fine control of the tool.

Through-the-arm control does not sufficiently reduce the inaccuracy of the robot arm in most cases. This leads to active or passive compliance end-effector control as alternative methods. Compliance refers to the tool's ability to compensate in particular axis when an error is present [18-22]; this is with out the intervention of the robot's position controller; it is solely dependent on the force control. In this situation, it is clear that a hybrid controller is non-existent, instead the force and position control are separate in active control, with integration occurring between the two. A natural compliance tool would also be suitable. However, in this research, the polishing tool was non-compliant; hence active compliance end-effector force control is favoured.

2.3 Passive/Active Compliance Control

In using an active or passive compliance end-effector, the device is mounted between the robot manipulator and the tool. The tool assembly (fixture) joining the tool to the machine or robot manipulator can therefore be considered the end-effector. An active or passive compliance end-effector control system involves the end-effector tooling having the ability to compensate in particular axes when a contact force error is present. Compliance can be understood as the degree or measure of ability the end-effector tooling possess to react to interaction forces [19]. As previously mentioned in the section, "Tool Fixture Design," of chapter 1, *active* refers to actuators making fine adjustments to the tool, while *passive* compliance is achieved without actuators by employing various mechanisms (links and springs). This is done without the intervention of the machine's position controller, and it is solely dependent on the force control. In other words, the force and position control are separate in active control allowing the active end-effector to give a better dynamic response.

Furthermore, active end effectors can be classified as programmable and non-programmable. The programmable type can accomplish trajectory polishing-force tracking, whereas the non-programmable active end effectors cannot. Hence, polishing force trajectories involving a varying force can be achieved. Most commercially available machines rely on active or passive force control normal to the surface being polished, as opposed to through-the-arm control. Examples include the Gintic SMART 3D Grinding and Polishing System [23,24], Polyem – polishing robot [14,25], and force control devices from PushCorp, Inc. [26].

With respect to this thesis research, the active end-effector approach was adopted, to take advantage of the characteristics mentioned above. With the active end-effector comes a possible modular, reusable design that also carries the enticing prospect of an end-effector for polishing being used on a variety of machines. (Both CNC and a wide variety of industrial robots could be equipped.)

2.4 Contact Modelling

The contact between the polishing tool and work-piece surface, during the polishing process, is an extreme case of the general abrasive wear that occurs on a soft metal surface abraded by hard sharp abrasive particles [27, 28]. The extreme case is known as abrasive friction. Kato examined abrasive wear resistance, abrasive wear modes, and abrasive wear rate [28]. Kato gives both 2-D and 3-D models of abrasive wear (on the microscopic level), as well as a formula for wear rate in each case, i.e., wear rate is equal to the wear volume divided by the sliding distance and the applied normal force. This derives from Archard's wear equation and of course, within this expression lies implicitly, shear flow stress. Material removal takes place when the accumulated plastic strain, in the deformed layer, reaches a particular critical value.

The authors, Ahn et al., of the research paper, "Intelligently Automated Polishing for High Quality Surface Formation of Sculptured Die,"[29] assert a contact model between fixed abrasive grains and a metal work-piece that considers the penetration depth of an abrasive, its average size and density, as well as the pressure applied on the work-piece surface and the work-piece hardness. They also used an acoustic emissions sensor to indirectly estimate the die surface roughness during the polishing process.

Zhang et al. performed an investigation of material removal in polishing with fixed abrasives [30]. There are other types of tools for surface polishing besides fixed abrasives; for example filamentary brushes and loose abrasives; however, their research (as well as the author's being presented) was confined to fixed abrasives, and acknowledges the presence to Hertzian stress at the surface of the work-piece being polished, for the particular geometry and materials involved. The contact between two bodies may be considered as Hertzian if the effect of friction is negligible, the contact is elastic, and the size of the contact region is small compared to the principal radii of curvature of the bodies at the contact [30]. Greenwood gives three approximate methods to calculating the Hertzian contact pressure/stress and contact area [31].

Concerning material removal rate, Zhang et al. also employ Archard's equation. Once again this did not involve the explicit use of shear flow stress. Research was previously undertaken to study the effects of pressure distribution on surface flatness, and indeed Zhang et al furthered this study by illustrating a parabolic material removal profile when the polishing force remains constant during automated polishing, for the Hertzian contact case.

2.5 Tool-Path Generation

There is a plethora of research devoted to tool path generation strategies, to achieve machining, grinding, and polishing [32-37]. In general, there are three types of techniques for tool path generation [32]: (1) the APT-based tool path method, (2) the Cartesian machining method, and (3) the Parametric machine method. Chung and Park [33] proposed a method of tool path generation from measured data – the physical work-piece is digitized and the measured data used to accomplish NC machining. While Lee et al. [14] use computer aided design (CAD) data or a developed CAM system called PolyCAM. Their PolyCAM method involves cutter contact (CC) data generation, cutter location (CL) data computation, and joint-value conversion based on the robot's inverse kinematics [14].

In all these various approaches, none consider the influence geometric data may have on process data (i.e. feed-rates, speeds and applied pressure or force) as in the case of automated polishing. That is, the radius of curvature of a part may, in some cases, affect the surface pressure during a finishing process, such as polishing.

2.6 Summary

This literary survey discusses the main type of machines available for automated polishing, the control techniques employed, previous contact modelling approaches, and tool path generation. The absence of force/pressure planning (or process data planning) based on geometric properties – mainly the principal radii of curvature, in any of the reviewed research, highlights the uniqueness of this thesis research.

CHAPTER 3: Contact Stress

Recalling the objective **to maintain a constant surface contact stress along a varying geometry surface** – the interaction between the polishing tool head and the work-piece surface must be considered; interaction refers to the polishing tool head pressing against the work-piece surface. An applied polishing force comes from the polishing tool head and pushes down on the work-piece surface, hence resulting in contact stress.

First, the basic theory of contact stress is introduced, which leads to the application of the Hertzian contact model. This model is established in terms of the work-piece geometry, and using numerical simulation, a contact stress distribution map is formed. (That is, the numeric simulation illustrates the contact stress primarily as a function of geometry.)

To simplify the calculations necessary to determine the contact stress, a cylindrical polishing tool with its axis of rotation normal to the work-piece surface is used. Additionally, it was assumed the friction torque is equivalent to the polishing torque necessary to remove material from the work-piece surface.

3.1 Basic Theory

Contact stress refers to the pressure (stress) arising from two bodies subjected to compressive loading by forcing them together, as shown in Figure 3.1. Contact stress is modelled to obtain a relationship between the applied force (the compressive load) and the maximum pressure (maximum compressive stress). In the isometric view on the left side of Figure 3.1, two semicircular disks are pressed together. Each disk has a maximum and a minimum principal radius represented by R_1 and R'_1 for disk 1, and R_2 and R'_2 for disk 2; disk 1 being above while disk 2 rests below.

The diagram on the right side in Figure 3.1 gives both the front elevation view and the plan view. This illustrates the maximum principal radius (in the front elevation view) and the minimum principal radius (in the plan view). In the front elevation view, overlapping profiles are used to indicate the displacement caused by the compressive loading.

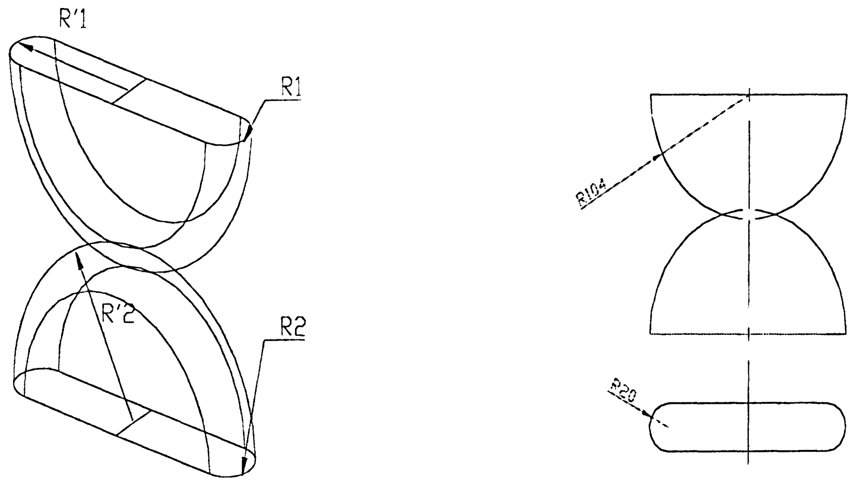

Figure 3.1 Two curved bodies pressed together

Both disks must be of an elastic material providing elastic deformation. Initially a point contact occurs at the instant the disks touch. It is through this point of contact that the applied compressive force passes. As the force increases, the point contact becomes surface contact, and will continue to increase with increasing force. This surface contact lies in a plane tangential to both curved surfaces of the disks at the initial point of contact; hence the line of action of the applied force is perpendicular (normal) to the contact surface plane, and it is for this reason that there is no friction force between the disk surfaces. The Figure 3.1 scenario of contact stress is known as Hertzian stress: because of the geometry of the two bodies, elastic deformation occurs in such a manner that the contact area changes as loading changes, thus the stress has a nonlinear relation with the applied force or load.

With this introduction to the theory of contact stress, one may now substitute disk 1 with the polishing tool head, while interpreting disk 2 as the work-piece; this is essentially how the contact stress model was developed. Of course, friction arises during polishing as the tool is rotating and being fed across the surface of the work-piece. This would be in a tangential direction and are essentially shear forces, which produce shear stresses. These shear forces are assumed to be responsible for removing the material being polished. However, based on previous research pertaining to material removal during polishing and abrasive wear (for metals) [27-30], either the Preston equation or the Archard equation is employed, and in these equations shear forces/stresses are implicit. Explicit shear stress values are not required to calculate material removal rate. Therefore, the normal stress remains the primary concern.

3.2 Contact Stress Model

In general, the contact area formed is elliptic [38]. The maximum pressure, i.e., the principal stress, occurs at the centre of the elliptic contact area and lies on the surface of contact. The principal stress on the contact surface is given as follows [38]:

$$\sigma_{zz} = -\left[\frac{M}{2}\left(\frac{1}{n} - n\right)\right]\frac{b}{\Delta} \tag{3.1}$$

where σ_{zz} is the compressive principal stress (indicated by the negative sign), and

$$M = \frac{2k}{k'^2\,E(k')}, \quad n = \sqrt{\frac{k^2 + k^2(Z/b)^2}{1 + k^2(Z/b)^2}}, \quad \Delta = \frac{1}{A+B}\left(\frac{1-\nu_1^2}{E_1} + \frac{1-\nu_2^2}{E_2}\right)$$

(See nomenclature for the denotation of the systems.)

The variable $k = \dfrac{b}{a}$, where a and b are the semi-major and semi-minor axis of the ellipse of contact, respectively, hence $k < 1$.

$$k' = \sqrt{1-k^2}$$

$E(k') = \int_0^{\pi/2} \sqrt{1-k'^2 \sin^2\theta}\; d\theta$, which is a complete elliptic integral of the second kind.

$$A = \frac{1}{4}\left(\frac{1}{R_1}+\frac{1}{R_2}+\frac{1}{R'_1}+\frac{1}{R'_2}\right) - \frac{1}{4}\sqrt{\left[\left(\frac{1}{R_1}-\frac{1}{R'_1}\right)+\left(\frac{1}{R_2}-\frac{1}{R'_2}\right)\right]^2 - 4\left(\frac{1}{R_1}-\frac{1}{R'_1}\right)\left(\frac{1}{R_2}-\frac{1}{R'_2}\right)\sin^2\phi}$$

$$B = \frac{1}{4}\left(\frac{1}{R_1}+\frac{1}{R_2}+\frac{1}{R'_1}+\frac{1}{R'_2}\right) + \frac{1}{4}\sqrt{\left[\left(\frac{1}{R_1}-\frac{1}{R'_1}\right)+\left(\frac{1}{R_2}-\frac{1}{R'_2}\right)\right]^2 - 4\left(\frac{1}{R_1}-\frac{1}{R'_1}\right)\left(\frac{1}{R_2}-\frac{1}{R'_2}\right)\sin^2\phi}$$

In addition to the above equations, the following also holds [38]:

$$\frac{B}{A} = \frac{(1/k^2)E(k') - K(k')}{K(k') - E(k')} = \frac{R'_1 + R'_2}{R_1 + R_2} \tag{3.2}$$

where $K(k') = \int_0^{\pi/2} \frac{d\theta}{\sqrt{1-k'^2 \sin^2\theta}}$, which is a complete elliptic integral of the first kind.

$$b = \sqrt[3]{\frac{3kE(k')}{2\pi}(F\Delta)} \tag{3.3}$$

3.2.1 Equation Manipulation and Application

Equation (3.2) is used to determine the value of k – the ratio of semi-minor axis to semi-major axis of the ellipse – and therefore k is a function of the ratio of B to A. As the ratio of B to A increases, the value of k decreases. Moreover, since both B and A are a function of the radii of curvature, k is ultimately a function of the radii of curvature as well; suffice it to say it is dependent on tool and part geometry. Upon the determination of k, the semi-minor axis b can be obtained by applying equation (3.3). With k and b determined, the semi-major axis can now be calculated if desired.

The polishing tool under study carries a flat polishing head, i.e. the polishing head is cylindrical with its axis of rotation normal to the part's surface. Therefore, its radii of curvature are taken to be infinite. The angle between the corresponding radii of curvature is also taken as zero ($\phi = 0$), and since the focus here is on the stress at the contact surface, $Z = 0$ and correspondingly $n = k$. For this situation equation (3.1) for maximum stress P_0 now becomes:

$$P_0 = \frac{b}{E(k')\Delta} \tag{3.4}$$

Observe that the ratio B to A now becomes:

$$\frac{B}{A} = \frac{R'_2}{R_2} \tag{3.5}$$

Since R'_2 is the maximum radius of curvature on the part while R_2 is the minimum, the ratio of B to A is always greater than unity. One may also infer that as the ratio of maximum radius to minimum radius of curvature increases, the contact region will become more elliptic.

3.2.2 Contact Stress Distribution

Furthermore, due to the stress being Hertzian and the contact area being elliptic, the stress also follows an elliptic distribution. Johnson [39] shows this distribution as a function of Cartesian coordinates x and y, where the coordinate frame's origin is concentric to the ellipse origin:

$$P_{seg}(x,y) = P_0[1-(x/a)^2-(y/b)^2]^{1/2} \tag{3.6a}$$

The maximum stress occurs at the centre of the ellipse while the stress is zero at the perimeter. Equation (3.6a) stems from the equation of an ellipsoid:

$$\frac{x^2}{a^2}+\frac{y^2}{b^2}+\frac{z^2}{c^2}=1 \tag{3.6b}$$

Here, the maximum contact stress is equivalent to 'c' (i.e., $c = P_0$), while 'z' represents the variation of stress at different x and y values (i.e., $z = P_{seg}(x, y)$). Substituting these values and rearranging to solve for $P_{seg}(x, y)$ gives equation (3.6a).

3.2.3 Mean Stress

Moreover, the mean stress across the elliptic contact area can be obtained by dividing the volume of the semi-ellipsoid by its elliptic area. This yields equation (3.6c):

$$P_m = \frac{2}{3}P_0 \tag{3.6c}$$

The user specified polishing pressure (stress) is considered as the mean stress. Also, the mean stress will be used in the following chapter (chapter 4) to calculate the elliptic friction torque.

3.3 Numerical Simulation

The above formulation of the contact model is numerically simulated using Matlab software (see Appendix-A1). Table 3.1 and Table 3.2 give the various properties of the polishing tool and the part respectively. The part material is steel. For a particular part, the radii of curvature of the part should correspond with the profile of the part as the tool moves across the part's surface. However, instead of being limited to one particular part, the simulation considered ranges of radii; in essence, this covers all possibilities. For each combination of radii, a range of applied polishing force may also be investigated. The applied polishing force, *F*, was taken from 2 N to 10 N.

Table 3.1: Tool properties

Description of property	Symbol of property	Value [units]
Tool diameter	d_t	10 [mm]
Maximum radius of curvature	R'_1	Infinity
Minimum radius of curvature	R_1	Infinity
Poisson's ratio	υ_1	0.15*
Young's modulus of elasticity	E_1	38000 [N/mm^2]*

* Value was based on previous research by authors Zhang et al., see reference 30

Table 3.2: Part Properties

Description of property	Symbol of property	Value [units]
Maximum radius of curvature	R'_2	Range of values are used
Minimum radius of curvature	R_2	Range of values are used
Poisson's ratio	υ_2	0.30
Young's modulus of elasticity	E_2	207000 [N/mm^2]

3.3.1 Contact Stress Mapping

Figure 3.2(a) illustrates the relationship between the maximum stress (P_0) and the radii of curvature (R_2 and R'_2) of the part; the applied force remained constant. It can be seen that the stress (pressure) is highest when the radii are smallest. In Figure 3.2(b), the elliptic contact area is illustrated to verify the stress graph. The elliptic contact area increases as the radii of curvature increases.

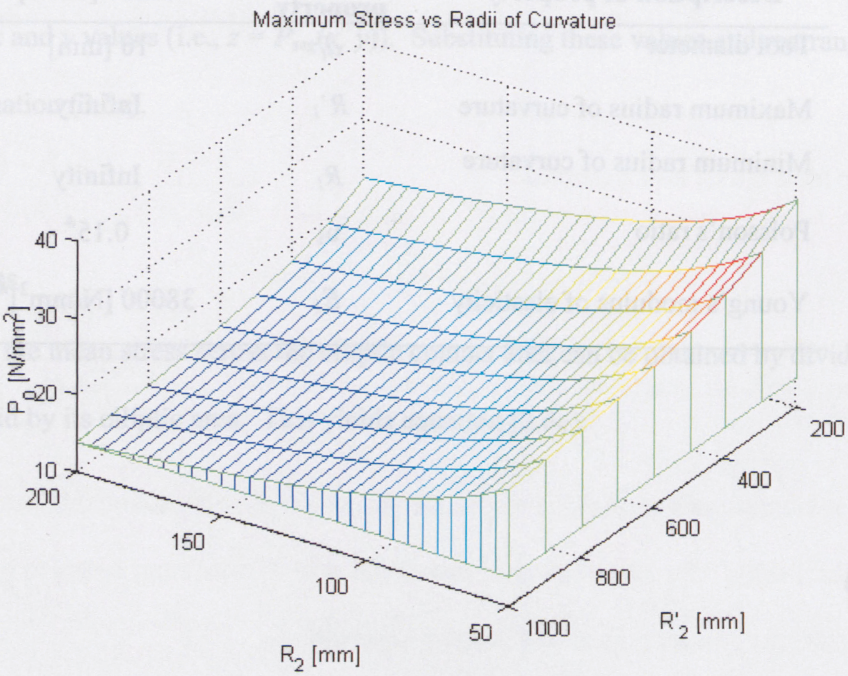

Figure 3.2(a) Variation in P_0 versus the radii of curvature

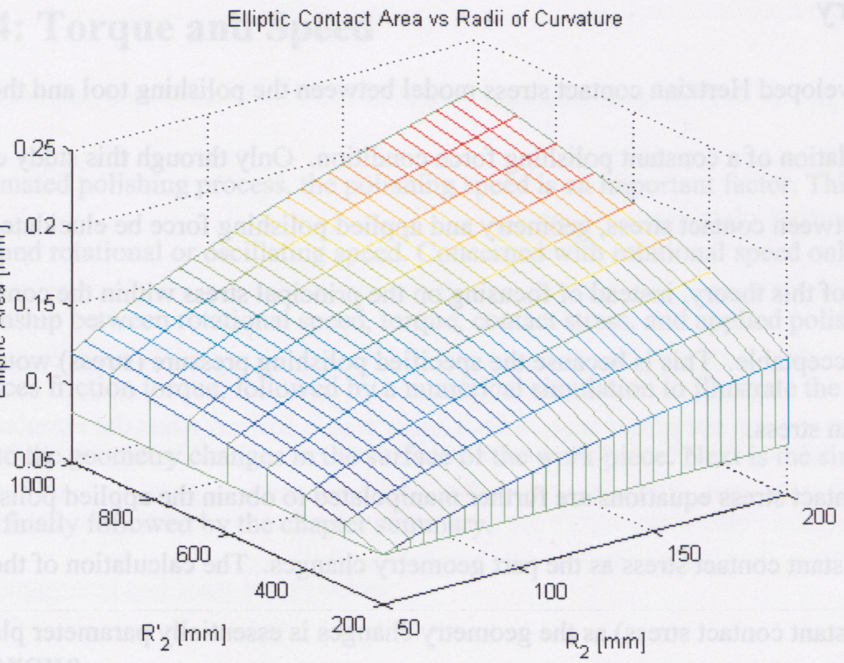

Figure 3.2(b) Variation of contact area versus the radii of curvature

3.3.2 Applied Force Calculation

The mapping of contact stress on the surface radii of curvature proves the applied force cannot remain constant, as is the case in Figure 3.2(a), but must be varied. By substituting equation (3.3) into equation (3.4), and solving for the force, one obtains a method for determining the force variations necessary for constant contact stress.

$$F = \frac{2\pi E^2(k')\Delta^2 P_0^{\ 3}}{3k} \tag{3.7}$$

3.4 Summary

The developed Hertzian contact stress model between the polishing tool and the part enables a numerical simulation of a constant polishing force condition. Only through this study can the relationships between contact stress, geometry and applied polishing force be elucidated. Pertaining to the application of this theory, instead of focusing on the principal stress within the contact area, the mean stress is more acceptable. This is because the specified polishing pressure (stress) would be considered as the desired mean stress.

The contact stress equations are further manipulated to obtain the applied polishing force required to maintain constant contact stress as the part geometry changes. The calculation of the applied polishing force (with constant contact stress) as the geometry changes is essentially parameter planning. This is discussed in detail in chapter 5, entitled, "Parameter Planning".

CHAPTER 4: Torque and Speed

In any automated polishing process, the polishing speed is an important factor. This includes both the tool's feed-rate and rotational or oscillating speed. Concerned with rotational speed only, this chapter will derive a relationship between rotational speed, torque, contact stress, and applied polishing force. The chapter first introduces friction torque, followed by a numerical simulation to illustrate the mapping of this friction torque to the geometry changes in the surface of the work-piece. Next is the simple derivation of rotational speed, finally followed by the chapter summary.

4.1 Friction Torque

Friction torque is the minimum quantity of torque resulting from the frictional forces between the polishing head and the part's surface opposing the tool's rotational motion. It was assumed the friction torque is equivalent to the polishing torque necessary to remove material from the work-piece surface.

Before delving into an in-depth discussion on friction torque and its relationship with contact stress, the basic theory is first addressed, and then followed by the non-Hertzian case, and finally the Hertzian contact scenario. In the non-Hertzian case, the pressure across the contact region was assumed constant to simplify the analysis, while the mean pressure was considered in the Hertzian case.

4.1.1 Basic Theory

The relationships between torque, pressure, area, applied force, as well as other parameters are provided. Generally (under constant radius and assumed uniform force distribution),

$$T_f = F_{sf}\, r \tag{4.1}$$

where $F_{sf} = F_s\, \mu_k$, $F_s = P A$. (See nomenclature.)

4.1.2 Non-Hertzian circular contact

The friction torque is first derived considering a non-Hertzian circular region as shown in Figure 4.1(a); this case refers to rubbing or friction wear, and there is no elastic deformation. As can be seen, the z-axis is positive coming out of the page. The contact area is formed when the circular flat polishing tool is in contact with a flat part. Therefore, the radius of the contact area is equivalent to the polishing tool head's radius. Since the tool is rotary, it revolves around the z-axis.

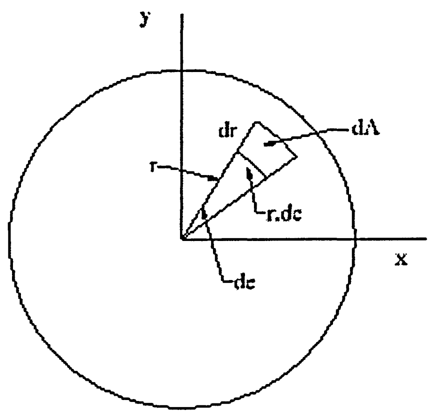

Figure 4.1(a). Diagram of circular contact area

The infinitesimal torque at the segment shown in Figure 4.1(a) is given as:

$$dT_f = P_{seg}\, dA\, \mu_k\, r \tag{4.2a}$$

where

$$dA = r\,dr\,de \tag{4.2b}$$

Substituting eqn. (4.2b) into eqn. (4.2a) yields the following equation:

$$dT_f = P_{seg}\, r^2\, dr\, de\, \mu_k \tag{4.3}$$

P_{seg} is assumed constant throughout for the non-Hertzian case, therefore, let P_s refer to the pressure (stress) across the entire non-Hertzian contact area. To obtain the torque across the circular contact area, eqn. (4.3) is double integrated and leads to the below:

$$T_f = \mu_k\, P_s \int_0^{2\pi}\int_0^{R} r^2 dr\, de = \mu_k\, P_s \frac{R^3}{3} \int_0^{2\pi} de = \frac{2}{3}\pi \mu_k P_s R^3 \tag{4.4a}$$

The first integral (the inner integral) gives the torque per unit radians, while the outer integral provides the total friction torque across 2π radians. From eqn. (4.4a), one sees that the friction torque is directly proportional to the contact stress and accordingly the torque would also be directly proportional to the applied polishing force, as shown below.

$$T_f = \frac{2}{3}\mu_k F_s R \tag{4.4b}$$

The friction forces due to the forward motion (feeding during the polishing) of the tool across the part are assumed small, and neglected.

4.1.3 Hertzian elliptic contact

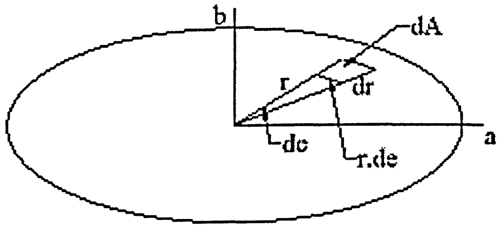

Figure 4.1(b). Diagram of the elliptic contact area

Focusing on Hertzian contact stress, in general cases the contact areas are elliptic. The first three equations (4.2a), (4.2b), and (4.3) used in the non-Hertzian contact scenario are applied. Since the focus is not on the pressure at particular locations within the elliptic contact area, but on the pressure over the entire elliptic contact area, the pressure at the infinitesimal segment, P_{seg}, is taken to be the same throughout the contact area. Therefore, P_{seg} is replaced with the average or mean pressure from eqn. (3.6c). This is applied to eqn. (4.3) to give equations (4.5) and (4.6) below.

$$dT_f = \mu_k P_m r^2 dr\, de \tag{4.5}$$

and

$$T_f = \mu_k P_m \int_0^{2\pi}\int_0^{R} r^2 dr\, de = \mu_k P_m \int_0^{2\pi} \frac{R^3}{3} de \tag{4.6}$$

Where for the elliptic region, R is the maximum radius at a particular angle e. R is a function of the angle between the semi-major axis and the direction of the radius, and it is expressed through the equation:

$$R^2 = a^2 \cos^2 e + b^2 \sin^2 e \tag{4.7}$$

Substituting eqn. (4.7) into eqn. (4.6) yields:

$$T_f = \frac{\mu_k P_m}{3} \int_0^{2\pi} (a^2 \cos^2 e + b^2 \sin^2 e)^{3/2} de = \frac{1}{3} \mu_k P_m \pi (a^3 + b^3) \tag{4.8}$$

and further manipulation to express torque as a function of force yields,

$$T_f = \frac{2}{9} \mu_k \pi (1 + 1/k) \times \left(\frac{3kF}{2\pi} \right)^{4/3} \times \left(E(k') \Delta \right)^{1/3} \tag{4.9}$$

Equation (4.8) and (4.9) complement equation (4.4) in that, for the Hertzian case, they also provide friction torque as a function of mean stress and applied polishing force, respectively.

4.2 Numerical Simulation

Once again, using Matlab software, a simulation generates graphs to elucidate the existing relationship between the elliptic friction torque and geometry; first under a constant force condition, and then under constant contact stress. The tool and part properties used in chapter 3 are used again.

4.2.1 Elliptic Friction Torque Mapping with Constant Force

This constant force scenario illustrates the friction torque behaviour that occurs naturally, i.e. without intervention from a force tracking control system. The elliptic friction torque is shown in Figure 4.2(a) to increase as the ratio of the maximum to minimum principal radius (R'_2 / R_2) increases. Chapter 3 demonstrated the relationship between k and the ratio R'_2 / R_2, and based on that, here it is clear that as the value of k decreases, and hence the difference between the semi-minor and semi-major axis increases (i.e., the contact area becomes more elliptic), the friction torque increases.

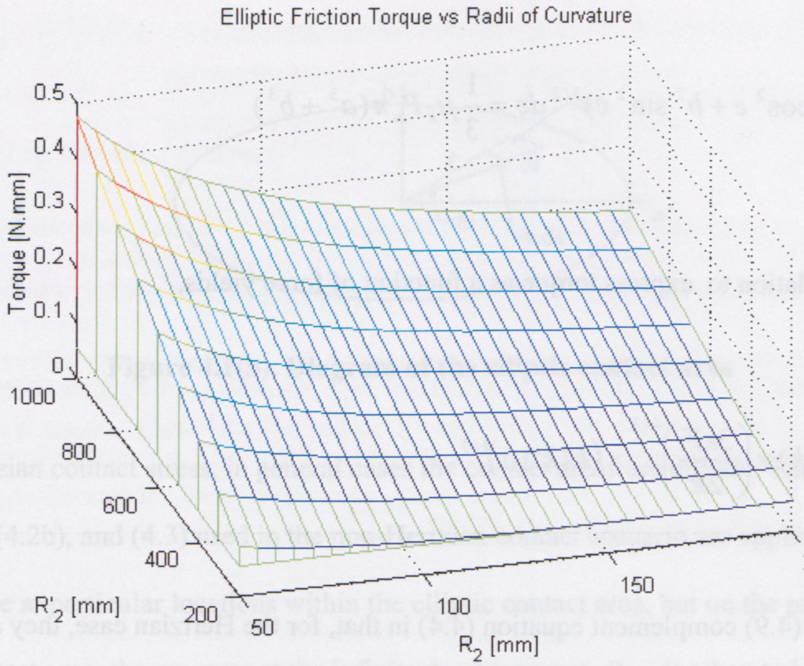

Figure 4.2(a). Graph showing the variation in T_f with the radii of curvature

To reaffirm this relationship, Figure 4.2(b) depicts a graph of ($a^3 + b^3$) versus the radii of curvature. A comparison is made between the graph of Figure 4.2(b) and that shown in Figure 3.2(a). Apparently, along the maximum principal radius of curvature axis the geometry of the contact ellipse has a stronger influence on the torque (see Figure 4.2(b)) than the contact stress does (see Figure 3.2(a)). Whereas along the minimum radius of curvature axis, the contact stress has a greater effect on the torque (see Figure 3.2(a)) than does the geometry of the contact ellipse (see Figure 4.2(b)). Because of this property, the largest contact area does not yield the largest quantity of torque. It is the most elliptic contact that will produce the highest torque.

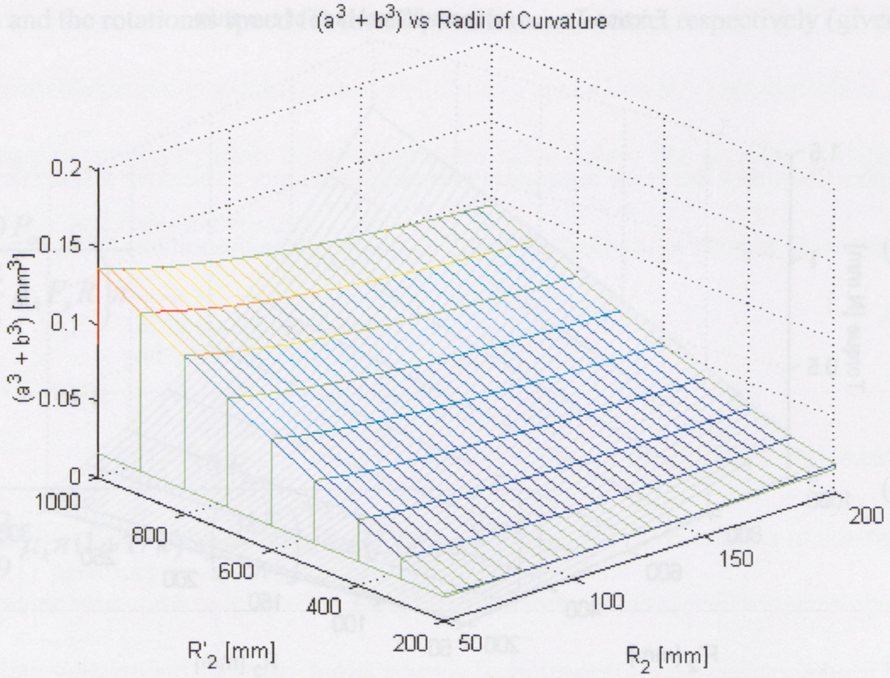

Figure 4.2(b). Graph showing the variation in ($a^3 + b^3$) with the radii of curvature at 2N

4.2.2 Elliptic Friction Torque Mapping with Constant Contact Stress

Figure 4.3, below, displays the changes in friction torque due to geometry changes, as the pressure remains constant. In this situation, as the contact region becomes less elliptic, i.e., the value of k increases, the friction torque increases.

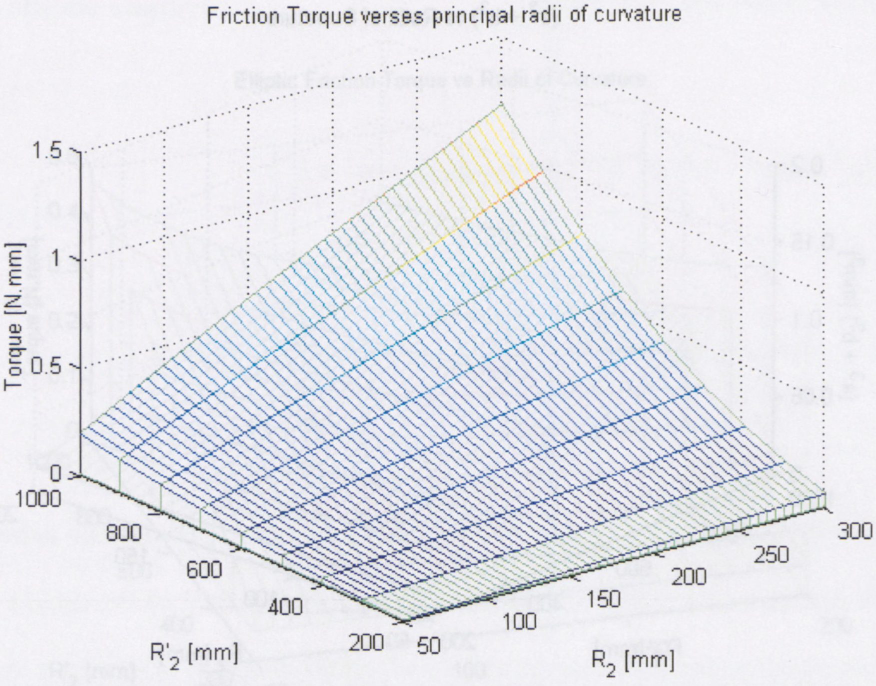

Figure 4.3. Torque versus radii of curvature at constant pressure setting

4.3 Rotational Speed

This section gives the relationship between the polishing tool's rotational speed and its torque. Investigating the effects of friction torque on the polishing speed is critical to achieving the goal of maintaining a constant speed throughout the polishing process. The mapping of friction torque to geometry has already been established, and can be easily applied here.

$$\omega = \frac{P_{out}}{T_R} \tag{4.10a}$$

where $T_R = I\dot{\omega} + T_f$ is the resultant torque.

This can easily be converted to revolutions per minute (RPM) by multiplying it with a conversion factor of $30/\pi$. Correspondingly, from eqn. (4.4b) and (4.9), the rotational speed for the non-Hertzian circular contact and the rotational speed for the elliptic Hertzian contact respectively (given in RPM) are obtained:

$$\omega_C = \frac{30 P_{out}}{\left(I\dot{\omega} + \frac{2}{3}\mu_k F_s R\right)\pi} \tag{4.10b}$$

$$\omega_E = \frac{30 P_{out}}{\left(I\dot{\omega} + \left\{\frac{2}{9}\mu_k \pi (1 + 1/k) \times \left(\frac{3kF}{2\pi}\right)^{4/3} \times \left(E(k')\,\Delta\right)^{1/3}\right\}\right)\pi} \tag{4.10c}$$

Both equations give speed as a function of varying force and geometry. However, for the non-Hertzian case the contact geometry and force would remain constant for the most part. Given the ability to adjust the power input, and hence the power output, the speed could be regulated to maintain a desired value.

4.4 Summary

With the conception of the contact stress model from Chapter 3 at hand, a relationship with the tool speed/torque is established and their distribution maps are also simulated in terms of the part geometry. Predicted values of friction torque and tool speed may now be obtained from the simulation, as the applied polishing force is varied to produce a constant contact stress on the work-piece surface.

CHAPTER 5: Parameter Planning

This chapter illustrates the force parameter planning necessary to achieve a specified constant contact stress (pressure). It gives a practical approach to applying the theoretical method introduced in Chapters 3 and 4.

5.1 Force/Pressure Planning

This approach to parameter planning is one of practicality, and assumes that path planning information already exist for the particular part to be polished. It is to give the reader an exposure and understanding of implementing the aforementioned contact stress model. This existing path planning information or data is acquired from the conventional or typical computer aided manufacturing (CAM) paradigm. Corresponding polishing force values, or in this case, pneumatic cylinder pressure values, since pneumatic cylinders actuate the polishing tool toward and away from the work-piece surface are augmented to the existing path planning data or G-code program.

5.1.1 Parameter Planning Process Overview

Figure 5.1 depicts the parameter planning process. The client G-code is read into the parameter planning program. Based on the path planning coordinates the theoretical applied polishing force and pneumatic cylinder pressure values are obtained. The pneumatic valve characteristics must at this point be considered. Valves have a delay in their response, and also posses a control frequency limit. That is, how frequent a control signal may be sent to the valve; at too high a frequency the valve will not respond. To the right of the process block pertaining to calculating the actual pressure and feedrate (see Figure 5.1), gives a possible method of compensating for delayed valve response. The subscript 'i' represents the current path planning coordinates (XYZ) and the corresponding tool orientation (A, B) and feedrate (F).

Notice the pressure parameter denoted by P_{i-j} also contains an addition subscript 'j'. (For the system used in testing 'P' represents pressure and not pause, as it usually is in G-code.) This algorithm produces a shift in the pressure parameter to allow compensation for valve delay. The variable 'j' depends on the extent of valve delay and control frequency.

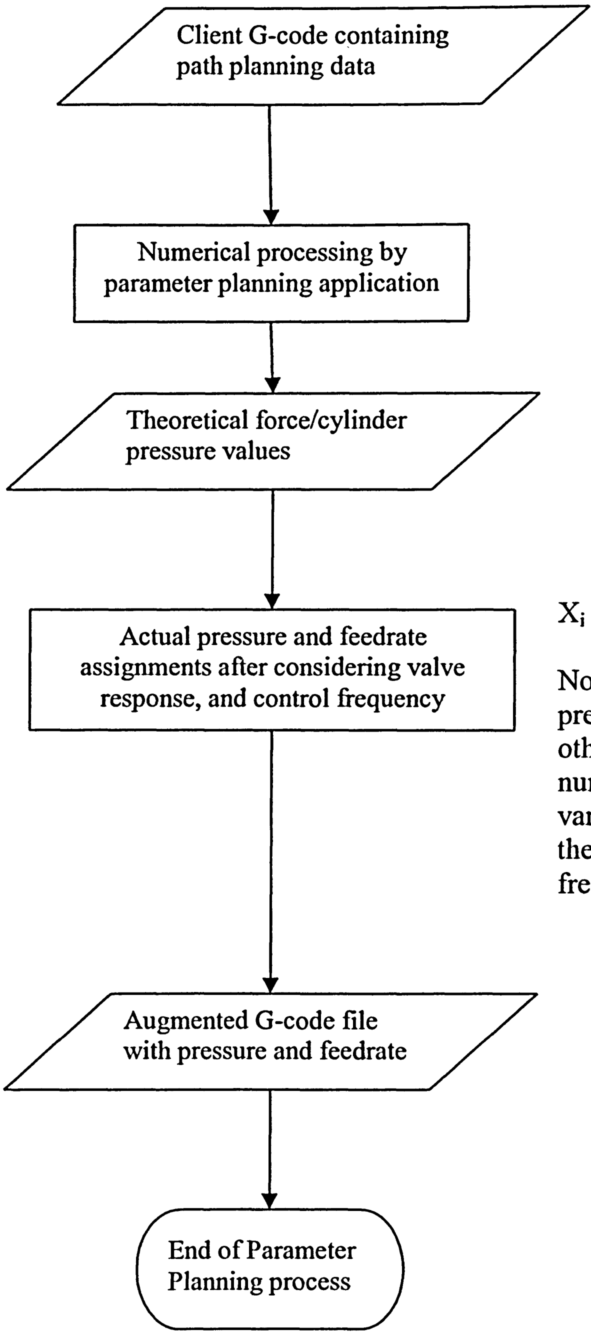

$X_i\ Y_i\ Z_i\ A_i\ B_i\ P_{i-j}\ F_i$

Notice by the subscript the pressure is not in sequence with the other parameters. It is offset by a number of terms, depending on variable j, which is a function of the valve response and control frequency.

Figure 5.1 Flow chart illustrating the parameter planning process

5.1.2 G-code Data Processing

For a detailed examination of the G-code file data processing, consider the part with a profile as depicted in Figure 5.2. This profile represents an edge of the part. Following the depiction is the G-code containing path planning data for polishing the edge of the part; however, the pressure planning data is missing.

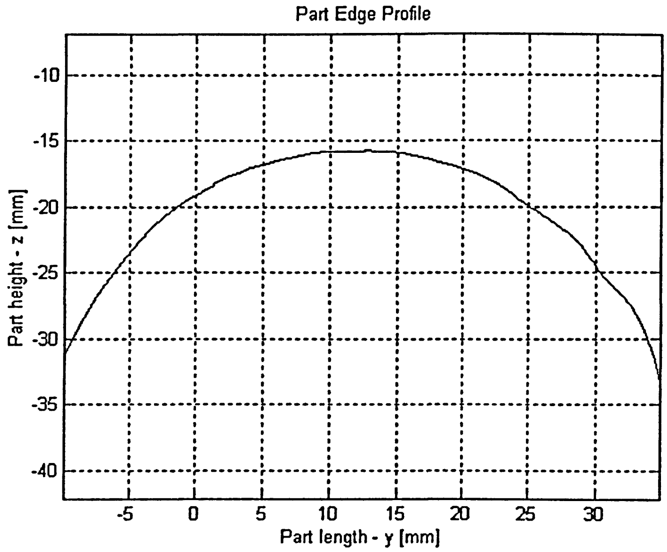

Figure 5.2 Work-piece Profile

Path planning data for the edge of the part:

N05	M03				
N10	G01	X26.501	Y27.149	Z-14.100	F5.0
N20	G01	X26.440	Y26.219	Z-13.834	F5.0
N30	G01	X26.379	Y25.289	Z-13.596	F5.0
N40	G01	X26.319	Y24.359	Z-13.420	F5.0
N50	G01	X26.258	Y23.429	Z-13.326	F5.0
N60	G01	X26.197	Y22.499	Z-13.282	F5.0
N70	G01	X26.136	Y21.569	Z-13.240	F5.0

The instantaneous radius of curvature is calculated for each XYZ coordinate. (Since the data is pertaining to the edge of the part, one of the radii of curvature is taken as infinity.) By either using the central difference method or a curve fitting technique, the radius of curvature is determined. The central difference method would be used to calculate the first and second-order derivatives. The equation for radius of curvature is given as follows:

$$R_2 = 1/Q(z) \tag{5.1}$$

where, $Q(z) = \dfrac{|z''|}{(1+z'^2)^{3/2}}$ and $z = f(y)$

Having calculated the radii of curvature at each path planning point, the applied polishing force was solved under constant contact stress conditions. With the applied force calculated, the pneumatic cylinder pressure is calculated and a new G-code file created. Below is an example of the pneumatic cylinder pressure augmented G-code (highlighted).

N05	M03							
N10	G01	X26.501	Y27.149	Z-14.100	A-14.3	B3.4	[redacted]	F1.0
N20	G01	X26.440	Y26.219	Z-13.834	A-12.1	B3.4	[redacted]	F1.0
N30	G01	X26.379	Y25.289	Z-13.596	A-9.9	B3.4	[redacted]	F1.0
N40	G01	X26.319	Y24.359	Z-13.420	A-7.9	B3.4	[redacted]	F1.0
N50	G01	X26.258	Y23.429	Z-13.326	A-5.9	B3.3	[redacted]	F1.0
N60	G01	X26.197	Y22.499	Z-13.282	A-3.9	B3.3	[redacted]	F1.0
N70	G01	X26.136	Y21.569	Z-13.240	A-1.9	B3.3	[redacted]	F1.0

During the polishing process, a control system would servo the cylinder pressure to achieve these desired values, which will result in a constant contact stress (pressure) along the part's surface. If the pressure requirements change during the polishing process, due to the surface roughness changing, the corresponding polishing parameters may easily be recalculated and inserted into the G-code for polishing once again.

5.2 Summary

This chapter provides a simple example of how the contact stress model theory can be applied to perform parameter planning, to correspond with already existing path planning. Pressure values are augmented into the conventional G-code to form a complete one for polishing. This new G-code is then executed by the polishing system.

CHAPTER 6: Dynamics and Control

Chapters 3 and 4 presented the contact model (workpiece-to-tool interaction) to provide an insight of the contact stress that can exist during a polishing process. Moreover, with Chapter 5 outlining the steps in applying the theoretical concepts of the earlier chapters to an actual part to achieve parameter planning, all that remains is the design and implementation of a control system.

However, before a model-based control system can be realized, one must develop a dynamic model of the polishing assembly (which is the end-of-arm tooling of the robot). From a control engineering interpretation, this dynamic model represents the plant; therefore, the accuracy of the model directly affects the efficiency of the control system. This present chapter stems from an appreciation of these effects, and so is also dedicated to producing an acceptable representation of the existing polishing tool and assembly that are being employed to perform the automated polishing. Following this is the design of an appropriate control scheme.

Since any dynamic model would be dependent on the existing physical system, the section immediately to follow provides an overview of the polishing system.

6.1 Automated System Overview

A brief description of the polishing system developed at Ryerson University is given – starting with the system hardware, and then the interaction between each hardware component.

6.1.1 Polishing System

This system consists of a hybrid robot and an active polishing end-effector. The robot has five axes, composed of a parallel kinematic machine known as a Parawrist Tripod (three axes) [40] and a gantry (two axes), as shown in Figure 6.1(a). The polishing tool assembly is attached to the moving platform of the robot (the end-effector). In the polishing assembly, there are three pneumatic cylinders equally spaced apart and attached to the lower and upper mounts, as shown in Figure 6.1(b). A pneumatic polishing spindle is held in the centre of these mounts.

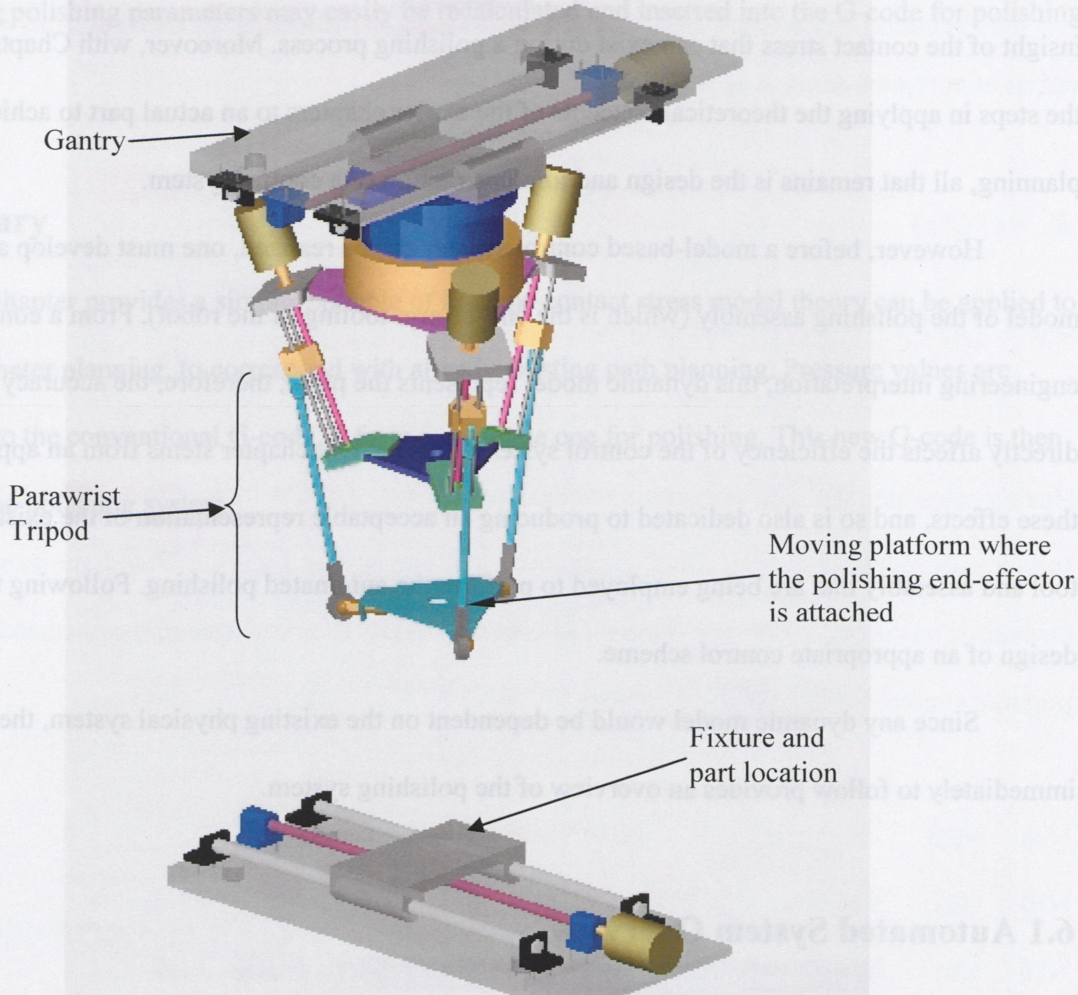

Figure 6.1(a). Automated polishing system

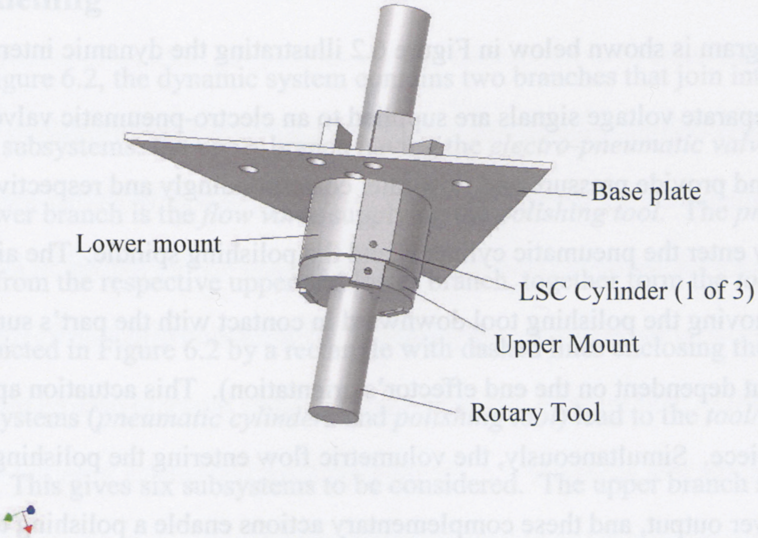

Figure 6.1(b). Polishing assembly attached to base plate

Figure 6.1(c) illustrates the polishing end-effector. By opening the chuck of the polishing tool (spindle), different polishing heads may be inserted to accommodate different part (work-piece) geometries. A cylindrical polishing head was used for this research.

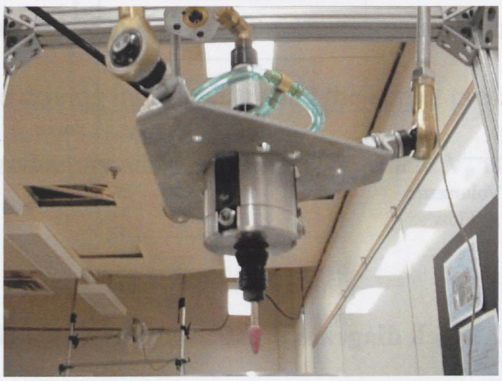

Figure 6.1(c). Actual assembly in the Ryerson University Lab

6.1.2 System Component Interaction

A block diagram is shown below in Figure 6.2 illustrating the dynamic interaction involved in this system. Two separate voltage signals are supplied to an electro-pneumatic valve and a flow valve to actuate the valves and provide pressure and flow rate; correspondingly and respectively, pressurized air and volumetric flow enter the pneumatic cylinders and the polishing spindle. The air pressure causes the pistons to extend, moving the polishing tool downward in contact with the part's surface (ideally in a normal direction, but dependent on the end effector's orientation). This actuation applies a polishing force on the work-piece. Simultaneously, the volumetric flow entering the polishing spindle provides (and dictates) a power output, and these complementary actions enable a polishing torque to be applied. Finally, based on the tool-to-workpiece interaction, a particular polishing pressure and spindle speed are obtained.

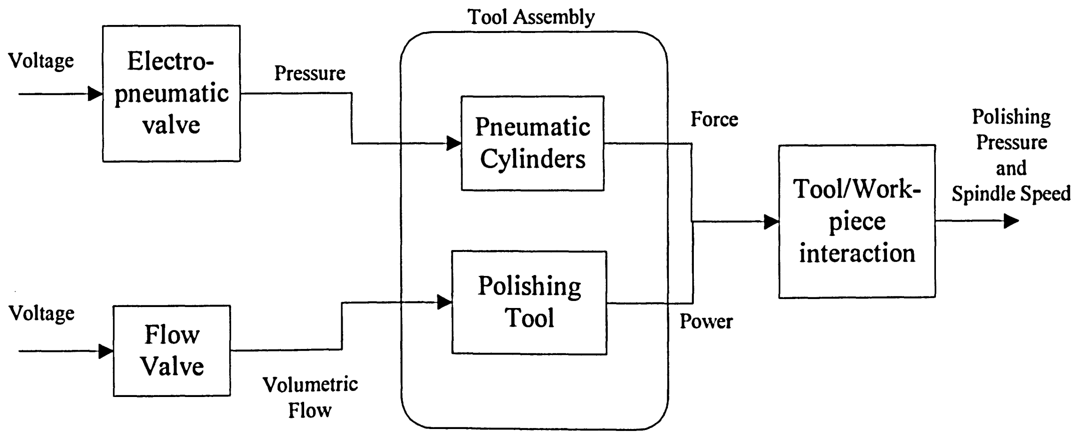

Figure 6.2 Block diagram illustrating the dynamic interaction

Adjusting the cylinder pressure permits variation in the applied polishing force, but this will also affect the spindle speed. Therefore, to maintain the desired spindle speed (or range of speed), the volumetric flow must also be adjusted. This coupling effect will be explained later in the chapter.

6.2 Dynamic Modelling

Referring to Figure 6.2, the dynamic system contains two branches that join into one. Each branch consists of two subsystems: the upper branch having the *electro-pneumatic valve* and *pneumatic cylinders*, while the lower branch is the *flow valve* supplying the *polishing tool.* The *pneumatic cylinders* and the *polishing tool* from the respective upper and lower branch, together form the *tool assembly* subsystem. This is depicted in Figure 6.2 by a rectangle with dashed lines enclosing the two subsystems. Finally, these two subsystems (*pneumatic cylinders* and *polishing tool*) lead to the *tool/work-piece interaction* subsystem. This gives six subsystems to be considered. The upper branch subsystems: *electro-pneumatic valve* and *pneumatic cylinder* will be considered initially, followed by the lower branch subsystems: *flow valve* and *polishing tool.* The *tool assembly* is then discussed, and finally the *tool-to-work piece interaction.*

6.2.1 Upper Branch Subsystems

(1) Electro-pneumatic Valve

The electro-pneumatic valve is used to supply pressure to the pneumatic cylinders. The transfer function of this valve is unknown, and because of this, the electro-pneumatic valve is treated as a "black box". The relationship between the driving input voltage and the output pressure will be based on the manufacturer's charts. For this introductory analysis, $P_c = G_p V_p$, where V_p is the voltage input variable and G_p is the transfer function.

(2) Pneumatic Cylinder

A dynamic model of the cylinder must now be derived to establish the necessary transfer function. The simple relationship between the force exerted by the cylinder, F_c, and its pressure, P_c, is given by:

$$F_c = P_c A_c \tag{6.1}$$

where A_c is the total cross-sectional area of the three pneumatic cylinders. In addition, the pneumatic cylinders enable compliance during the polishing process; this is similar to having a spring between the polishing tool and robot's end-effector. However, the compliance is only normal to the surface of the work-piece, and hence the cylinder pistons are pushed in the retraction direction as reaction forces increase, and then return to their initial position as reaction forces return to desired magnitudes. An increase in the force on the tool assembly (i.e. the reaction force) originates from the work-piece and robot when position inaccuracies in the polishing process occur.

It should be noted that the reaction forces do not always return to their desired magnitudes and therefore the cylinder pressure must be adjusted appropriately to restore the original magnitude of the applied polishing force.

By considering the control volume bounded by the cylinder and piston as shown in Figure 6.3, the compliance of the cylinder may be modelled. The control volume is enclosed by the rectangle with dashed lines.

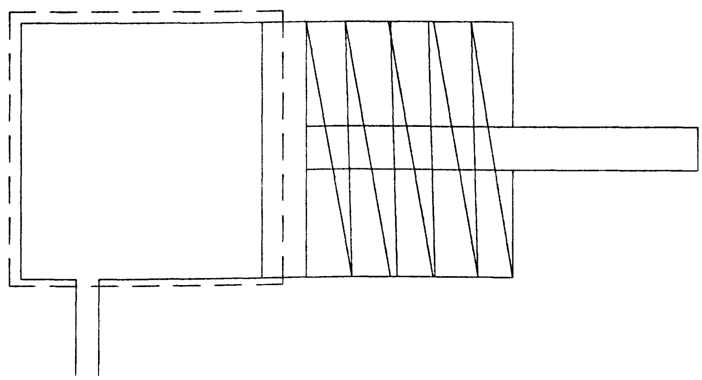

Figure 6.3 Cylinder modelled with control volume methodology

The expansion and reduction of the volume in the pneumatic cylinder is assumed to be a reversible adiabatic process of an ideal gas [41]. No heat is transferred to or from the fluid (i.e. the air in the cylinder) during the expansion or reduction process. The density of air within the cylinders determines the degree of compliance of the polishing tool assembly (the end of arm tooling); in essence the density can govern the stiffness of the polishing assembly. For an adiabatic process in which air is taken to be an ideal gas, the pressure-to-density relationship, P-ρ, is given by:

$$P_c = C\rho^{\gamma} \tag{6.2}$$

The cylinder friction is negligible during expansion or compression; C is a constant, ρ is the air density in the cylinder, while $\gamma = c_p/c_v$ at temperature, T_c. The specific heat capacity at constant pressure and constant volume are respectively represent by the symbols c_p and c_v. Since $\rho = m/V$, equation (6.2) can further yield a pressure-to-volume relationship with the case of the mass of air in the cylinder (or the pneumatic circuit) being constant.

$$\Delta P_c = C' / \Delta V_c^{\gamma} \tag{6.3}$$

C' is now the new constant resulting from the product of the mass of air raised to the power of γ, multiplied by C. The changes in cylinder volume cannot be predicted or controlled, and equation (6.3) is taken to represent disturbances in the system. As mentioned in the preceding paragraphs, this disturbance ultimately originates from position inaccuracies that cause fluctuations in the reaction force on the polishing assembly.

Both equations (6.1) and (6.3) are used in the dynamic modelling of the system. Furthermore, when the two subsystems (the electro-pneumatic valve and the pneumatic cylinder) are combined, P_c =

G_pV_p is substituted into equation (6.1), along with consideration to the pressure disturbances expressed in equation (6.3), it yields:

$$F_c = (G_pV_p + \Delta P_c)A_c \tag{6.4}$$

6.2.2 Lower Branch Subsystems

The following section discusses the subsystems that compose the lower branch, see Figure 6.2: the flow valve and polishing tool.

(3) Flow Valve

The flow valve in the system will control the amount of volumetric flow going to the polishing tool, therefore determining the power out of the tool. This valve is controlled or driven by an electrical signal (voltage or current) and the relationship between voltage and flow rate will be initially based on the manufacturer's charts. This is the same approach adopted from the electro-pneumatic valve modelling, and at this moment the flow valve is treated as a "black box"; hence $q = G_qV_q$, where V_q is the voltage input variable and G_q is the transfer function relating V_q and q.

(4) Polishing Tool – Power input and output

The power input of the pneumatic tool must be considered and one can start with the familiar relation:

$$P_{in} = F\,V$$

P_{in} is the power input to the pneumatic polishing tool (spindle), F is force and V represents velocity. In the case of the spindle, the force is a product of pressure multiplied by the cross-sectional area of the intake port to the spindle, one can write the above power equation as follows:

$$P_{in} = (p_s - p_x)\, A_x\, V$$

where p_s represents the supply pressure, p_x is the exhaust pressure, and A_x is the cross-sectional area. The exhaust pressure is the output pressure from the spindle. As well, volumetric flow, q, is the product of the cross-sectional area and the velocity, and hence:

$$P_{in} = (p_s - p_x)\, q \qquad (6.5)$$

The power input is equal to the pressure drop across the spindle times the volumetric flow through the spindle. Also note, there exists another relationship between the pressure drop across the polishing tool and the volumetric flow through it. This relation is given as:

$$R_f = (p_s - p_x)/q \qquad (6.6)$$

The resistance of the fluid flow within the pneumatic spindle, R_f, is the pressure drop across the spindle divided by the volumetric flow through the spindle. Rearranging equation (6.6) to obtain the pressure drop, and then substituting this equation into equation (6.5) yields:

$$P_{in} = R_f\, q^2 \qquad (6.7)$$

Now consider the power output of the tool. This was given in Chapter 4 – equation (4.10a). This power output will be less than the power input, due to the polishing tool's less than 100% mechanical efficiency. Now when the efficiency of the polishing tool, eta (η), is included the equations are as follows:

$$P_{out} = \eta P_{in}$$

$$P_{out} = T_R \omega = \eta R_f q^2$$

After rearranging the above equation to obtain the torque, the torque output of the spindle is related to the angular velocity by:

$$T_R = \frac{\eta R_f q^2}{\omega} \tag{6.8}$$

When the two subsystems –the flow valve and the polishing tool – are joined together, the torque becomes a function of the input voltage and angular speed. Correspondingly $q = G_q V_q$ is substituted into equation (6.8) to yield:

$$T_R = \frac{\eta R_f G_q^{\,2} V_q^{\,2}}{\omega} \tag{6.9}$$

With an equation for the torque output of the polishing tool derived, the equation of motion pertaining to the polishing head may now be derived. By summing the force moments about the polishing head's rotating axis, i.e., the z-axis, and interpreting clockwise moments as positive, gives way to the following:

$$I\dot{\omega} + T_f = T_R \tag{6.10}$$

where 'I' denotes the moment of inertia of the polishing head, '$\dot{\omega}$' denotes the angular acceleration.

(5) Tool Assembly

The polishing tool assembly was previously depicted in Figure 6.1(b) and 6.1(c) of the "6.1.1 Polishing System" section. Figure 6.4, shown below, now gives a tool assembly diagram illustrating the important forces of the system.

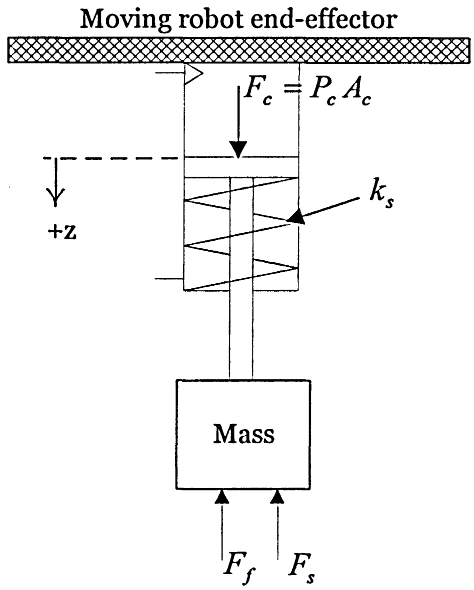

Figure 6.4 Tool assembly diagram

From Figure 6.4, one can now derive the equation of motion for the entire assembly – the pistons, polishing tool and other components – which are all represented by the mass shown. The displacement, z, is relative to the cylinder's body or housing (or moving robot end-effector since the cylinder is rigidly attached to the end-effector). It is not relative to the machine's base (i.e., the global coordinate system).

The reaction force from the work-piece and the kinetic friction force arising between the moving components are denoted with the symbols F_s and F_f respectively; the symbol k_s represents the spring constant or stiffness of the spring within the pneumatic cylinder. This spring provides a spring return force for the single-acting cylinder.

Referring to the diagram (Figure 6.4), initially the equation of motion is as follows:

$$M\ddot{z} = P_c A_c - 3(k_s z) - F_s - F_f \tag{6.11}$$

The term '$k_s z$' is the force from the spring. It is multiplied by a factor of 3 because there are three cylinders to consider. Also, note that the kinetic friction force of the system, F_f, is the damping force in this dynamic system.

The acceleration would originate primarily from disturbances and errors in tracking the profile of the specific work-piece during the polishing process. The disturbance or error leads to an increase or decrease in the applied polishing force, and if large enough can cause an acceleration in the z-direction relative to the robot's end-effector (as shown in Figure 6.4). In reality, there is static friction in the assembly, and therefore force disturbances in the system will not always cause a z-direction displacement. Aside from this, the acceleration resulting would be brief, random and very difficult, if not impossible, to measure. It would most likely appear as sharp fluctuations in the torque and pressure measurements during the polishing operation. This suggests designing a robust system able to handle this disturbance. The inertia force is neglected due to these factors.

In addition, gravitational effects are ignored; this is because the equilibrium position of the mass was selected to be the point of reference for z-displacement, and occurs at the zero volume position when the cylinder is fully retracted. Furthermore, when the cylinders are pressurized a new equilibrium position is available; hence for every cylinder pressure set point there exist an equilibrium position. Since the main goal during the polishing process is to maintain an equilibrium static state between the applied force F_c (due to pressure P_c) and the reaction force F_s, the equilibrium point was chosen to correspond to a specified cylinder pressure set point. This eliminates the spring return force from the analysis.

Since static equilibrium is desirable and may be challenged by disturbances and errors as mentioned above, the static friction of the polishing assembly now contributes a significant effect and must be included. Rewriting equation (6.11), and with equation (6.4) also being substituted gives,

$$(G_p V_p + \Delta P_c) A_c + F_{fs} = F_s \tag{6.12}$$

The static friction force is denoted by F_{fs}. The reaction force of the system, F_s, along with the geometry of the work-piece, gives the frictional torque acting on the polishing spindle. This is explained in the next section to follow.

(6) Tool-to-Workpiece Interaction

The tool-to-workpiece interaction was discussed in-depth in Chapter 4, "Torque and Speed". The derived equations are repeated for convenience as follows,

$$T_f = \frac{2}{3}\mu_k F_s R \tag{4.4b}$$

and

$$T_f = \frac{2}{9}\mu_k \pi (1 + 1/k) \times \left(\frac{3kF_s}{2\pi}\right)^{4/3} \times \left(E(k')\Delta\right)^{1/3} \tag{4.9}$$

The applied force, which can be taken to be the same as the reaction force, F_s, is supplied from equation (6.12), and substituting this equation into the above equations (4.4b) and (4.9) yields:

$$T_f = \frac{2}{3}\mu_k\left[(G_pV_p + \Delta P_c)A_c + F_{fs}\right]R \tag{6.13}$$

$$T_f = \frac{2}{9}\mu_k\pi(1+1/k)\times\left(\frac{3k\left[(G_pV_p + \Delta P_c)A_c + F_{fs}\right]}{2\pi}\right)^{4/3}\times\left(E(k')\,\Delta\right)^{1/3} \tag{6.14}$$

The same equations and methods used in chapter 3 apply when calculating the geometric variations of the part's profile, for solving eqn. (6.14).

6.3 System Modelling

The preceding dynamic equations describe a multiple input multiple output (MIMO) system, and may be arranged in a matrix form to represent the dynamic system. The matrix equation below depicts this – with the inputs being the voltage signals for the electro-pneumatic valve and the flow valve, V_p and V_q^2, respectively; and the outputs being the cylinder pressure, P_c, and the angular acceleration, $\dot{\omega}$.

$$\begin{bmatrix} P_c \\ \dot{\omega} \end{bmatrix} = \begin{bmatrix} G_p & 0 \\ -\dfrac{2\mu_k R G_p A_c}{3I} & \dfrac{\eta R_f G_q^{\,2}}{I\omega} \end{bmatrix} \cdot \begin{bmatrix} V_p \\ V_q^{\,2} \end{bmatrix} \tag{6.15}$$

This pertains to the non-Hertzian polishing scenario, as the bottom row of equation (6.15) was obtained by substituting equations (6.9) and (6.13) into equation (6.10), and then solving for the angular acceleration.

Note: The resultant torque output, T_R, is approximately equal to the friction torque, T_f.

The model ignores the static friction and pressure disturbances (ΔP_c) considering the nominal system only. During testing, the control system can be tuned to compensate for static friction and pressure disturbances. Although the matrix equation (6.15) is not in state-space form, it does illustrate an existing coupling between the input, V_p and V_q^2, and the angular acceleration output. Also apparent is the nonlinear nature of the system.

6.3.1 Feedback Signals

For a closed-loop control system, a pressure/force sensor and rotational speed sensor may be used to feedback the output signals. A force sensor is ideal, since there is friction in the polishing assembly; relying on pressure measurements to provide the actual value of the applied polishing force introduces an element of error. With either pressure or force sensor, the measured values may be compared with the desired values obtained from parameter planning.

Let H_p denote the transfer function of the pressure sensor, H_f – the force sensor's transfer function, and H_w denote the transfer function of the rotational speed sensor. So for the pressure/force the transfer function is no longer G_p, but as given below:

$$\frac{P_c}{V_p} = \frac{G_p}{1 + G_p H_p} \tag{6.16a}$$

$$\frac{F_s}{V_p} = \frac{G_p A_c}{1 + G_p A_c H_f} \tag{6.16b}$$

6.3.2 Feedback Linearization

Consider both the system's coupling and non-linearity; equation (6.15) is similar to the companion form (or controllability form), i.e. $\dot{\mathbf{x}} = f(\mathbf{x}) + \mathrm{G}(\mathbf{x})\mathbf{u} \quad \mathbf{y} = \mathbf{h}(\mathbf{x})$ [42], but not exactly. It does however apply to the bottom row of the matrix equation (6.15), where:

$\dot{\mathbf{x}} = \dot{\omega}$ a scalar quantity

$\mathbf{u} = \begin{bmatrix} V_p & V_q^{\,2} \end{bmatrix}^T$

$\mathbf{y} = \omega$ a scalar quantity

$f(\mathbf{x}) = 0$

$$G(\mathbf{x}) = \begin{bmatrix} -\dfrac{2\mu_k R G_p A_c}{3I} & \dfrac{\eta R_f G_q^{\,2}}{I\omega} \end{bmatrix}$$

So a feedback linearization approach for a MIMO system is adopted, and this in fact leads back to matrix equation (6.15) being the desired form. For this approach, allow

$$\mathbf{E}(\omega) = \begin{bmatrix} \dfrac{G_p}{1+G_pH_p} & 0 \\ -\dfrac{2\mu_k R G_p A_c}{3I} & \dfrac{\eta R_f G_q^{\,2}}{I\omega} \end{bmatrix}$$

$$\mathbf{y}' = \begin{bmatrix} P_c \\ \dot{\omega} \end{bmatrix} \qquad \mathbf{u} = \begin{bmatrix} V_p \\ V_q^{\,2} \end{bmatrix}$$

Technically the output $\mathbf{y}$ is differentiated until the inputs appear, and this is partially the case, but because a linear system (that really needs no input-output linearization) is being combined with a nonlinear system that does, the notation $\mathbf{y}'$ is used instead of $\dot{\mathbf{y}}$. Hence,

$$\mathbf{y}' = \mathbf{E}(\omega)\mathbf{u} \tag{6.17}$$

$$\mathbf{v} = \begin{bmatrix} v_1 \\ v_2 \end{bmatrix} = \begin{bmatrix} P_c \\ \dot{\omega}_d - k_1 e_1 \end{bmatrix} = \begin{bmatrix} P_c \\ \dot{\omega} \end{bmatrix}$$

where $e_1(t) = \omega(t) - \omega_d$ and is the tracking error. Here is where the rotational speed sensor can be incorporated; like the pressure sensor, it too is used to compare the actual rotational speed of the spindle with the desired speed.

6.3.3 Decoupling

Due to the coupling nature of the system, the matrix **E**(ω) is known as the coupling matrix and its matrix inverse $\mathbf{E}^{-1}(\omega)$ is called the decoupling matrix. The feedback linearization can be performed by using the new input as follows:

$$\mathbf{u} = \mathbf{E}^{-1}\mathbf{v} = \mathbf{E}^{-1}\begin{bmatrix} v_1 \\ v_2 \end{bmatrix} \tag{6.18}$$

Equation (6.18) is known as the decoupling control law and when it is substituted into equation (6.17), the input **v** now directly affects the output $\mathbf{y}'$, and hence the system is decoupled, as well as linearized.

As alluded to in a previous paragraph, there exists a tracking error between the desired speed and actual speed. All that remains in the control scheme design is to design an acceptable, stable tracking error response. The following equation, $\dot{e}_1 + ke_1 = 0$, governs the tracking error response and is a typical first order differential equation with the solution $-e_1(t) = e_1(0)e^{-kt}$. Please note lowercase italic '*e*' without the subscript represents the exponential function (i.e., the inverse of the natural logarithm). Therefore the response will approach zero asymptotically as the time, *t*, approaches infinity.

When undergoing the process of tuning the control system, to adjust and obtain a more appropriate or desirable response, the k-value may be varied to suit.

6.4 Summary

This chapter presented a dynamic model of an active end-effector, and proposed an appropriate control scheme. The scheme portrays a unique MIMO system comprising of both linear and nonlinear portions. The coupling and nonlinear nature of the dynamic system was also emphasized and resolved; a decoupling matrix and feedback linearization were employed to achieve this.

CHAPTER 7: Experiment

The verification of scientific or engineering theory is of utmost importance along the path of transfer – the theoretical to the physical or applicable. Presented thus far, in the preceding chapters, was an engineering theoretical development with the purpose of achieving the first steps of automated polishing.

This chapter presents experiments designed to facilitate verification, starting with testing for the response in the electro-pneumatic valve, and then verifying the positive effects of polishing parameter planning (chapter 5: Parameter Planning), by means of open-loop testing.

7.1 Valve Response

The polishing tool was under no load during this test. Control signals with various characteristics – frequency, amplitude, step input - were sent to the electro-pneumatic valve, while simultaneously measuring the response via a pressure sensor. This was an experiment to measure the response time of the valve, and hence determines an appropriate operating bandwidth of the control signal.

For the electro-pneumatic valve, voltage was the input signal. According to the manufacturer's charts this signal should be in one-to-one relation with the output pressure of the valve, hence – 1 V should produce 1 bar.

A cross-correlation was performed on the two series of data – the control signal and the response signal. To follow are graphs depicting the input and response, as well as the cross-correlation.

Figure 7.1 illustrates the step response to a 2 bar input. Upon first glance, the valve may appear to be a first order system, but when one examines the initial 0.1 seconds of the response, the slight dip in the curve indicates a higher order system. Moreover, the precise pressure response is too quick to be precisely measured by the pressure sensor, and therefore no overshoot or oscillation has been depicted on the graph.

From Figure 7.1, the final settling value is on average 2.1 bars. The rise time is approximately 0.11 seconds, and the settling time approximately 0.2 seconds*. The steady-state error appeared to be on average 0.1 bars (1×10^4 Pa).

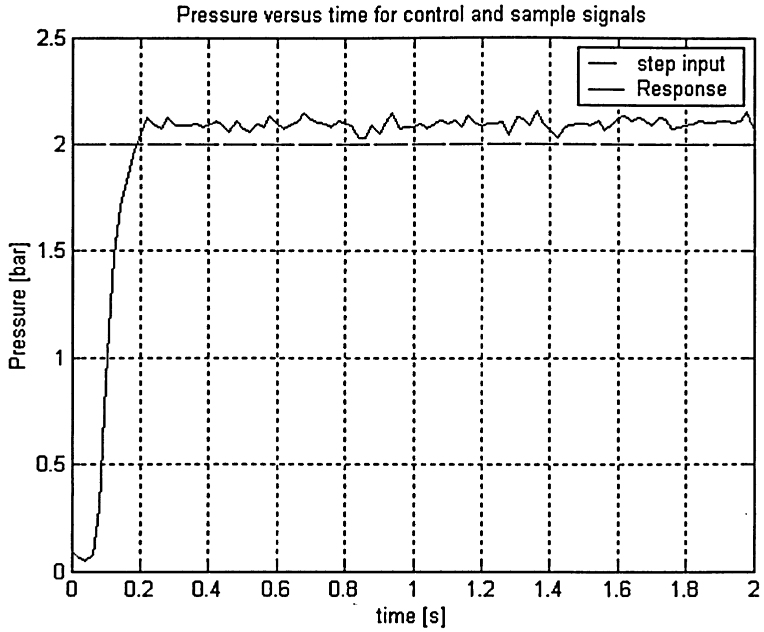

Figure 7.1 2 bars step input response

The remaining graphs depict a sinusoidal input signal and its corresponding response, followed directly below by a cross-correlation function plot. The control signal (input signal) frequency was varied from 0.5 Hz to 5 Hz, as well as varying the amplitude from 0.5 bars to 1.5 bars, with the sample frequency constantly held to 50 Hz.

Performing the cross-correlation on both signals (control and response) for each test, displays the cross-correlation at various time lags; for this testing each lag interval represents 0.02 seconds. Figure 7.2 illustrates this and indicates that at a control frequency of 1 Hz, the highest correlation is obtained for a lag of 5; a lag of 5 is equivalent to 100 ms (milliseconds). Even when the amplitude was varied at this particular frequency the lag remained the same.

* The plus or minus 2% approach, of the final settling value, was used to calculate the settling time.

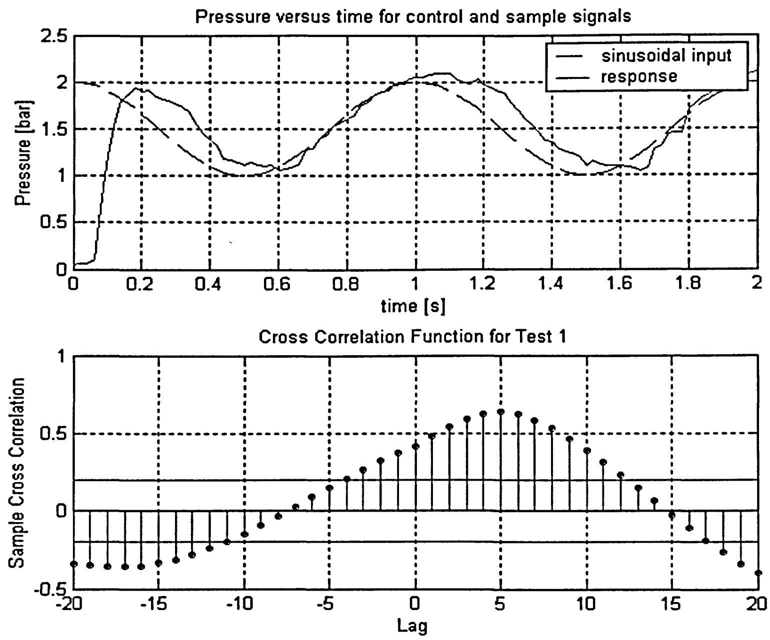

Figure 7.2 Pressure-response and cross correlation function for Test 1: Control frequency – 1 Hz, amplitude – 0.5 bar

One should also notice that in the above Figure 7.2 the time delay or lag in the response to the input control signal is not constant. This characteristic is a product of the physical structure of the system. The pressure in the system must be exhausted through the electro-pneumatic valve, and so there will always be a delay in pressure drop whenever the control signal attempts to lower the system pressure. However, when the control signal is increased in attempt to raise the system's pressure, the pressure response closely follows.

Several tests were performed and are presented in the appendix. As one would expect, as the control frequency is increased from 0.5 – 5 Hz, the response deteriorates and can no longer be used (see Figure 7.3). It was found that a control frequency of 1 Hz is most appropriate, and will be employed for further experiments.

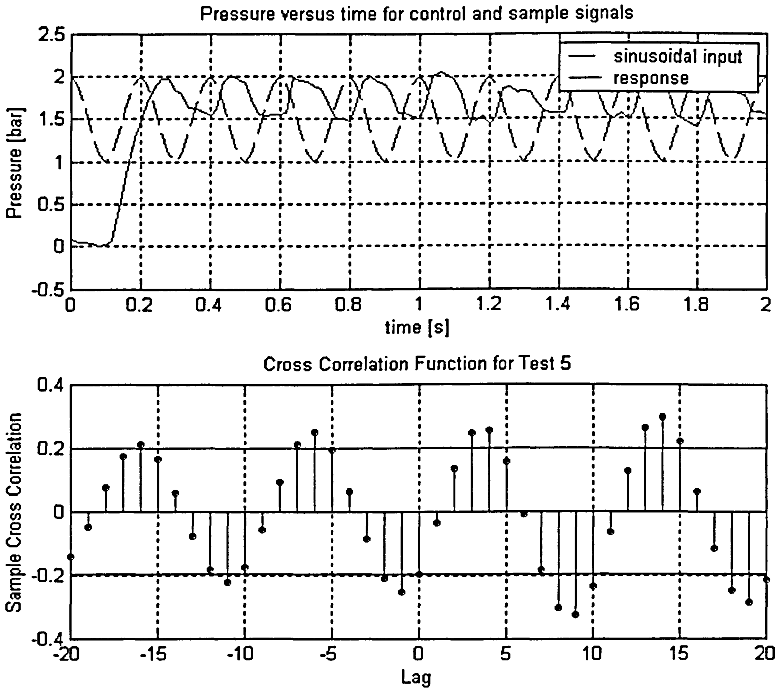

Figure 7.3 Pressure-response and cross correlation function for Test 5: Control frequency – 5 Hz, amplitude – 0.5 bars

7.2 Experiment Description

A number of metal parts were prepared. These parts had similar geometry and their profile was measured using a 2-D laser profile scanner (Cobra 2D from Optical Gaging Products Inc.). Polishing was performed with and without the application of the pressure planning. The parts' profiles were then re-measured to look for changes. The idea was to test for changes in the part's profile after polishing was done; one part with the parameter planning applied while the other without. The scanning machine's accuracy is 10 micrometers in the Z-direction; the height of the part is in the Z-direction. The dynamic resolution is 1.0 micrometers. The below Figures 7.4(a) and 7.4(b) display the Cobra 2D Laser Profile Scanner and its data acquisition software, called Scan X.

Figure 7.4(a) Cobra 2D Laser Profile Scanner

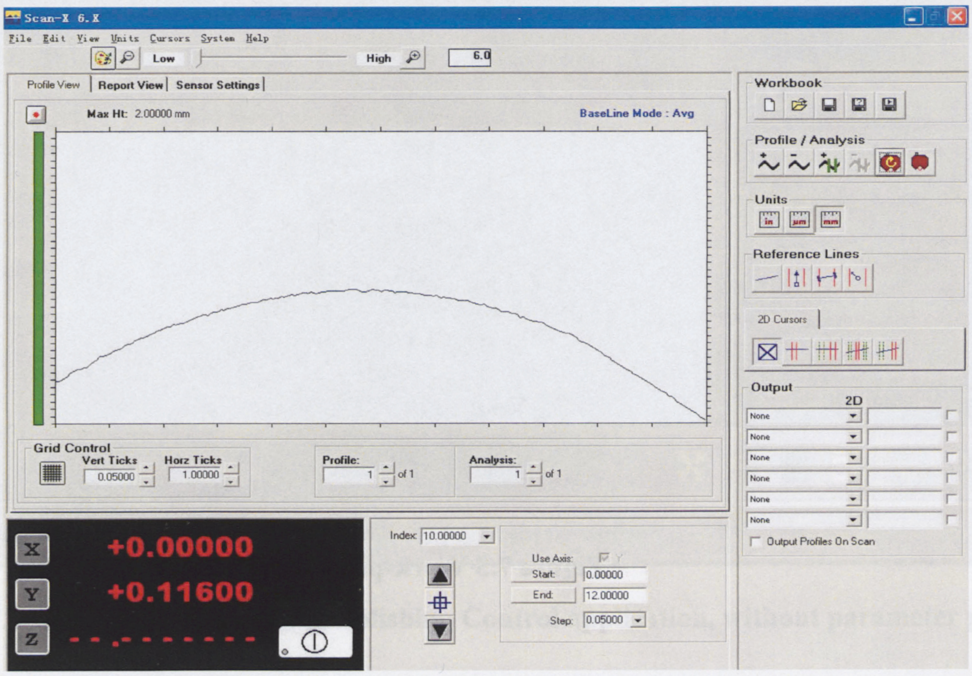

Figure 7.4(b) Data acquisition software – Scan X

The experiment considers polishing the edge of the part only (see the above Figure 7.5), and so it becomes a 2-D scenario. A conventional G-code file pertaining to the edge of the part was read into the parameter planning program (see appendix A1.2). The program generates the required tool orientation and cylinder pressure for each path planning point. It first refits the part's edge; based on the position coordinates supplied in the G-code, the program applies a polynomial curve fitting technique (least squares approximation). Then for each coordinate position, the corresponding maximum and minimum radius of curvature was calculated. Of course, because the edge of the part is being polished, one of the radii of curvature is always infinite. The knowledge of the radii of curvature enables the determination of the necessary force required to maintain a specified polishing pressure. With the force data obtained from the polishing parameter planning, the pneumatic cylinder pressure was calculated to match the particular path along the edge being polished. The parameter planning program finally augments the cylinder pressure data (as well as the tool's orientation), to the original G-code, forming a new augmented G-code file. Here are the G-codes for both scenarios (i.e. with and without parameter planning).

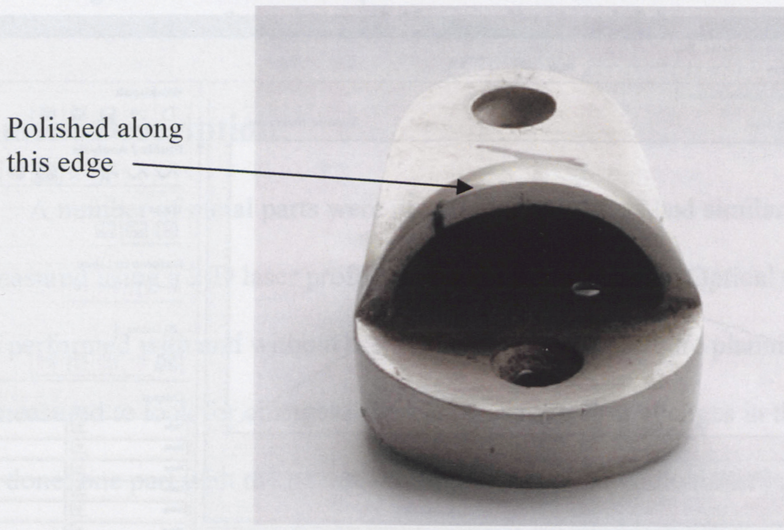

Figure 7.5 Work-piece

Figure 7.6(a) depicts the augmented G-code without the use of parameter planning. The pneumatic cylinder pressure is held constant at 2.25 bars in the G-code. However, with an observed steady-state error of -0.1 bars under loaded conditions, the constant pressure was approximately 2.15 bars. In Figure 7.6(b), the parameter planning method is utilized, and this is evident by the varying pneumatic cylinder pressure, from 1.71 bars to 2.30 bars (the error being ±0.1 bars).

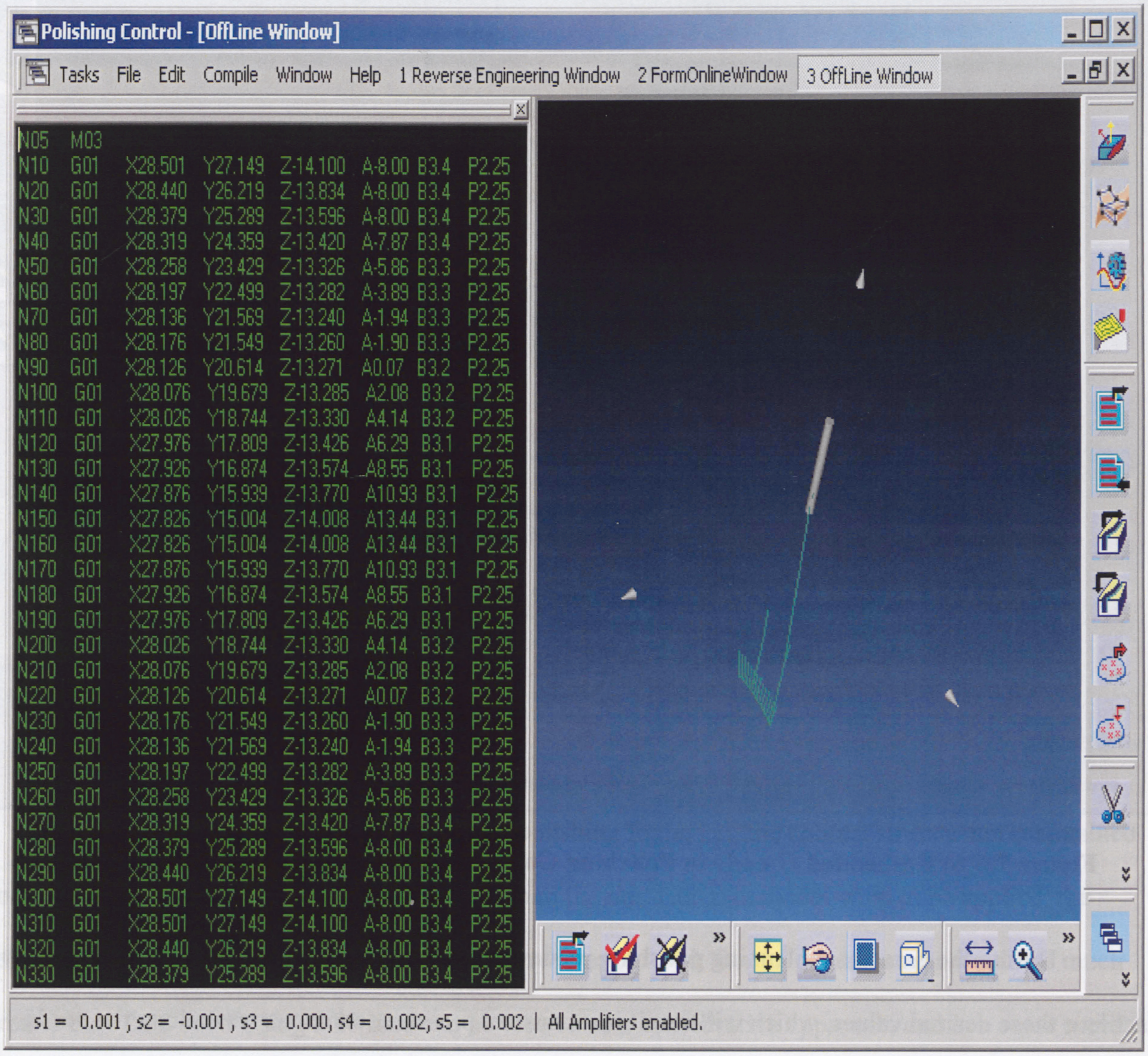

Figure 7.6(a) Embedded G-code in Polishing Control application, without parameter planning

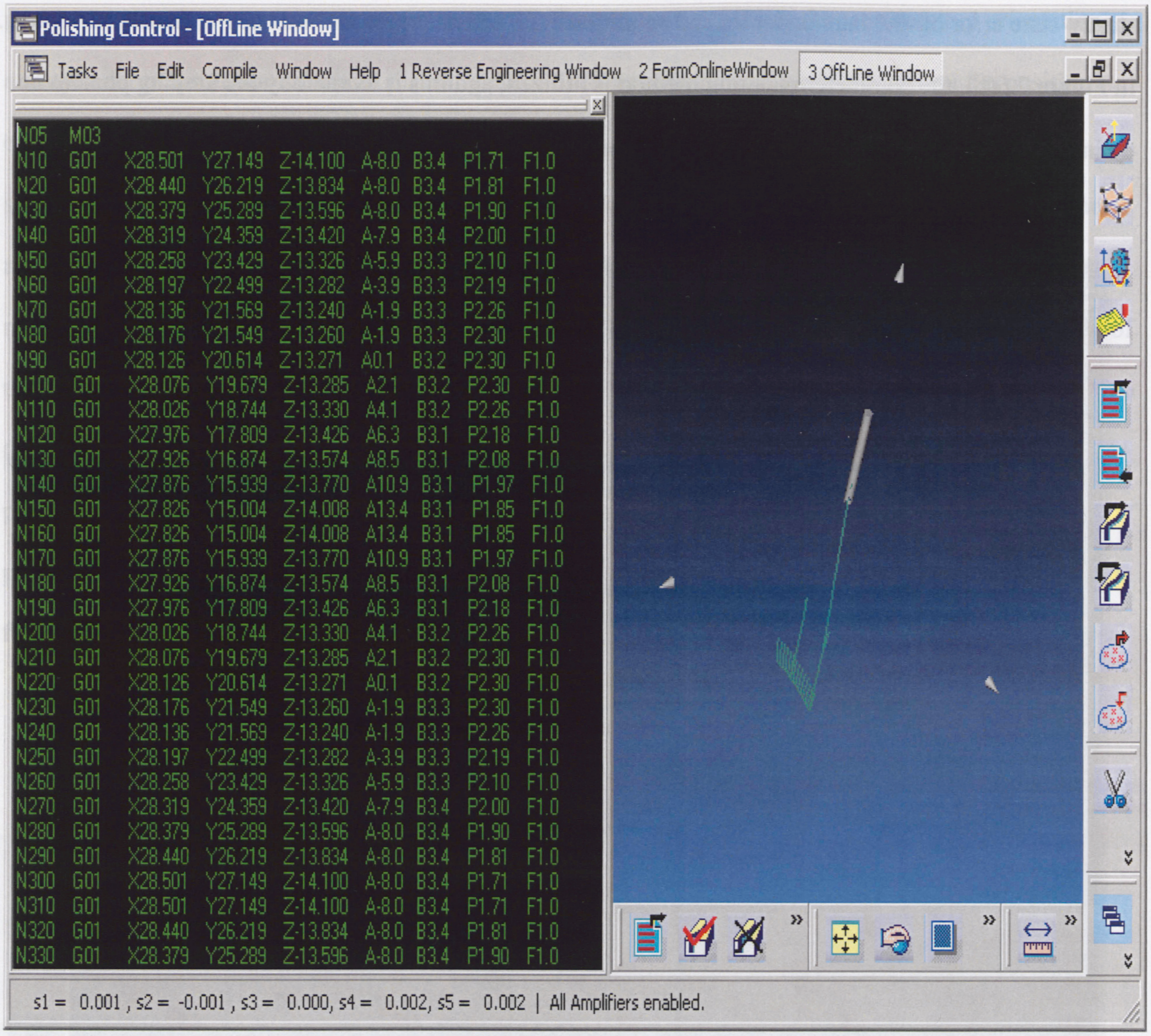

Figure 7.6(b) Embedded G-code in Polishing Control application, with parameter planning

During the parameter-planning polishing process a control system servos the cylinder pressure to achieve these desired values, which will result in a constant pressure (contact stress) along the part's surface. The range of pressure, 1.71 bars to 2.30 bars, is according to a 50 N/mm^2 desired surface contact stress. The 2.30 bars is required when the polishing tool reaches the top of the arc (refer to Figure 7.5), while the 1.71 bar value is required when polishing the end of the arced edge. Figure 7.7 shows the experiment in progress.

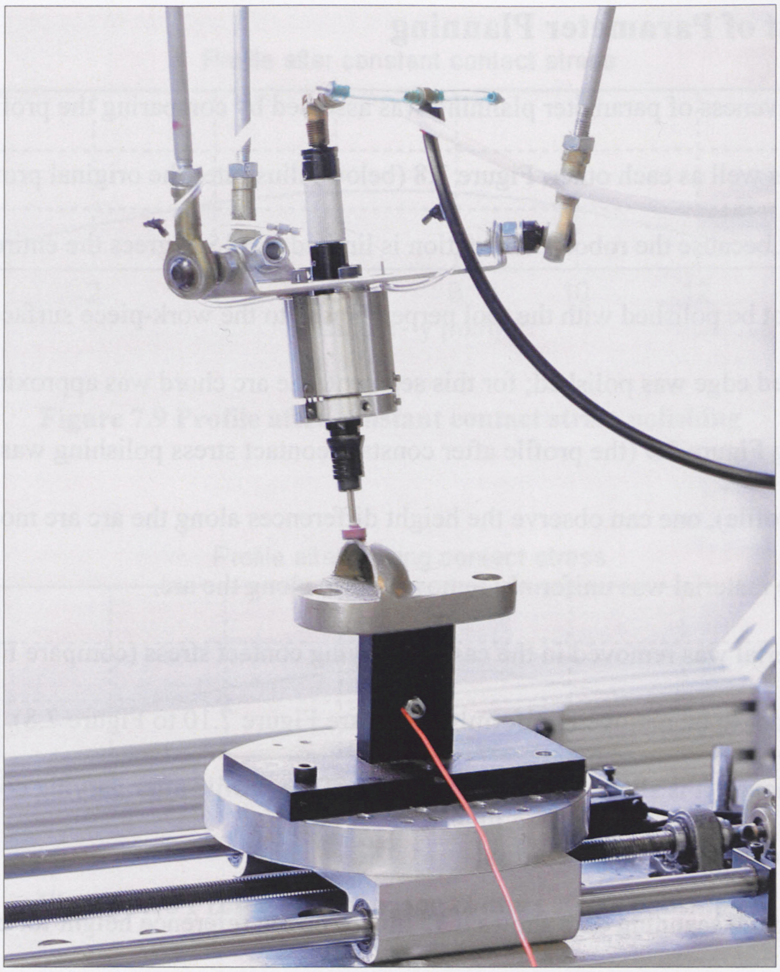

Figure 7.7 Experiment running in the Robotics and Manufacturing Automation Laboratory (RMAL)

For the scenario of applying a constant polishing force, i.e., the contact stress is not maintained constant, if the work-piece geometry is ignored and the non-Hertzian model were to be applied, the resulting applied force/cylinder pressure necessary to apply a 50 N/mm^2 contact stress would be much greater than 2.25 bars. Using 2.25 bars can be viewed as a conservative approach, and in a sense more realistic; one does not expect a manufacturer to apply a significantly damaging stress on the work-piece, to perform Automated Polishing. Moreover, due to the low control frequency – as determined in the value response experiment – and the small increments of motion used in the path planning (0.1 mm), the feedrate was set to 0.1 mm/s. This made the polishing process rather slow.

7.3 Assessment of Parameter Planning

The effectiveness of parameter planning was assessed by comparing the profiles of the each part with the original, as well as each other. Figure 7.8 (below) illustrates the original profile of the edge polished. Note that because the robot's orientation is limited to ±15 degrees the entire edge shown in Figure 7.5 could not be polished with the tool perpendicular to the work-piece surface. Hence, only a segment of the arced edge was polished; for this segment, the arc chord was approximately 15 mm long.

Comparing Figure 7.9 (the profile after constant contact stress polishing was performed) to Figure 7.8 (the original profile), one can observe the height differences along the arc are more or less the same. In other words, the material was uniformly removed from along the arc.

More material was removed in the case of varying contact stress (compare Figure 7.10 to Figure 7.9), and it seems not to be removed uniformly (compare Figure 7.10 to Figure 7.8). What is also noticeable, even though it is slight, is the steeper slope of the profile after varying contact stress polishing than the profile after constant contact stress.

Examining the scanning data shows 0.35 mm to be the reference height for each profile. The maximum heights of the profiles for the original, constant contact stress, and varying contact stress are 1.24 mm, 1.31 mm, and 1.56 mm, respectively.

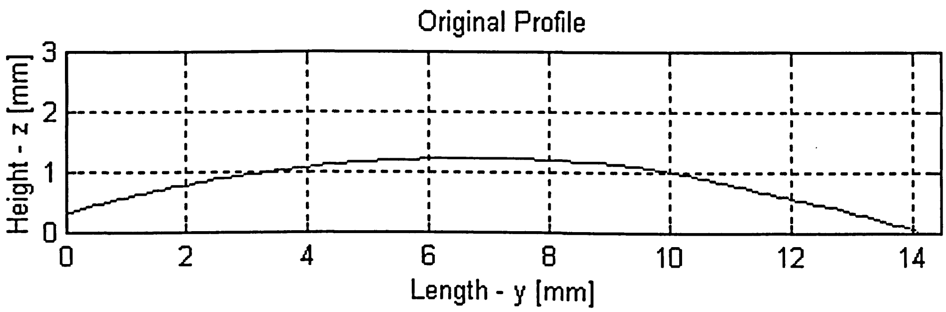

Figure 7.8 Original segment profile

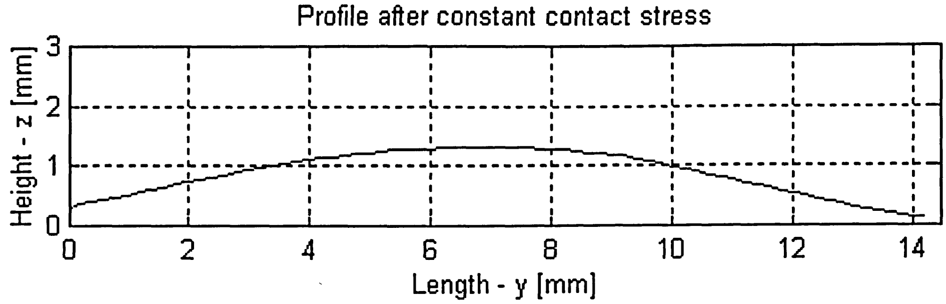

Figure 7.9 Profile after constant contact stress polishing

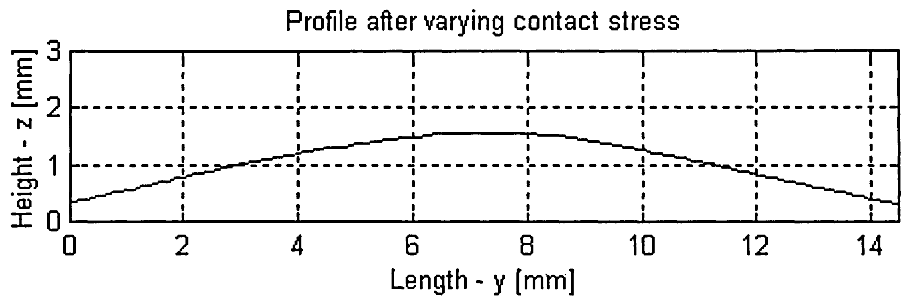

Figure 7.10 Profile after varying contact stress polishing

Figure 7.11 provides a bird's eye view or plan elevation of the polished parts. On the left side is the varying contact stress case (i.e., the pneumatic cylinder pressure remained constant throughout). A deep impression was left at the end of the arc segment, as depicted within the circle. This is partially due to angular misalignment during the polishing process, as one can see that for each work-piece the left side is slightly larger than the right side. However, in the case of varying contact stress, the increased contact stress also plays an influential role in forming the impression. Moreover, the region polished is both wider and longer for the varying contact stress scenario than for the constant contact stress scenario. More tool markings occur with the varying contact stress case as well.

From the aspect of preserving the original profile of the part, the most important feature of the arc segment is its radius of curvature. The following graph (Figure 7.12) compares the radius of curvature of each part, while Table 7.1 illustrates the percentage change from the original profile for each case.

Moving along the arc's chord in 1 mm increments, the radius of curvature of the part profile pertaining to the constant contact stress is always closer to the original radius of curvature; except at the 13 mm chord length.

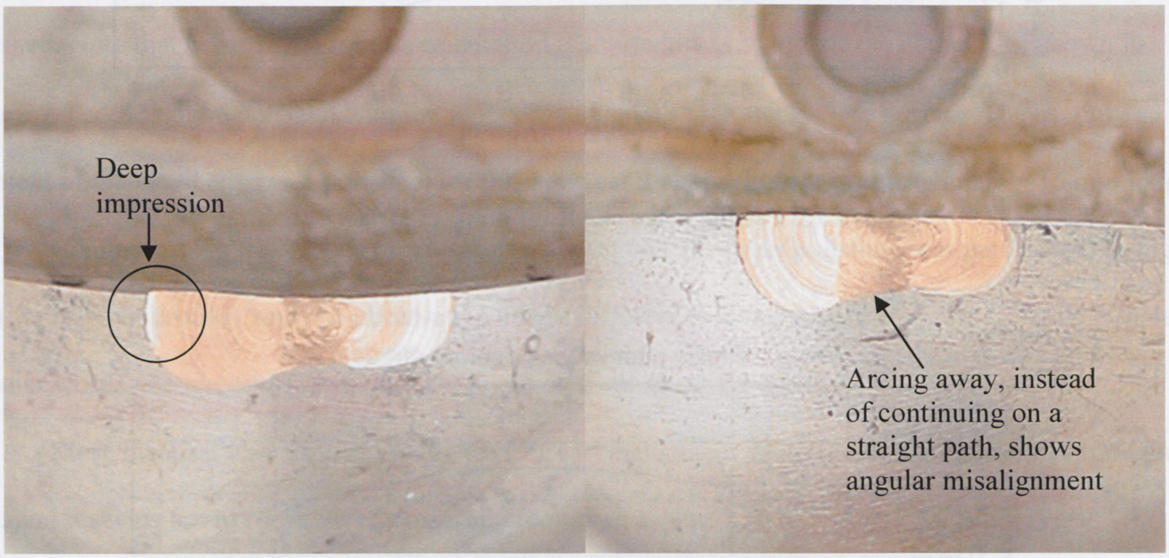

Figure 7.11 Work-pieces after polishing: varying contact stress (left), constant contact stress (right)

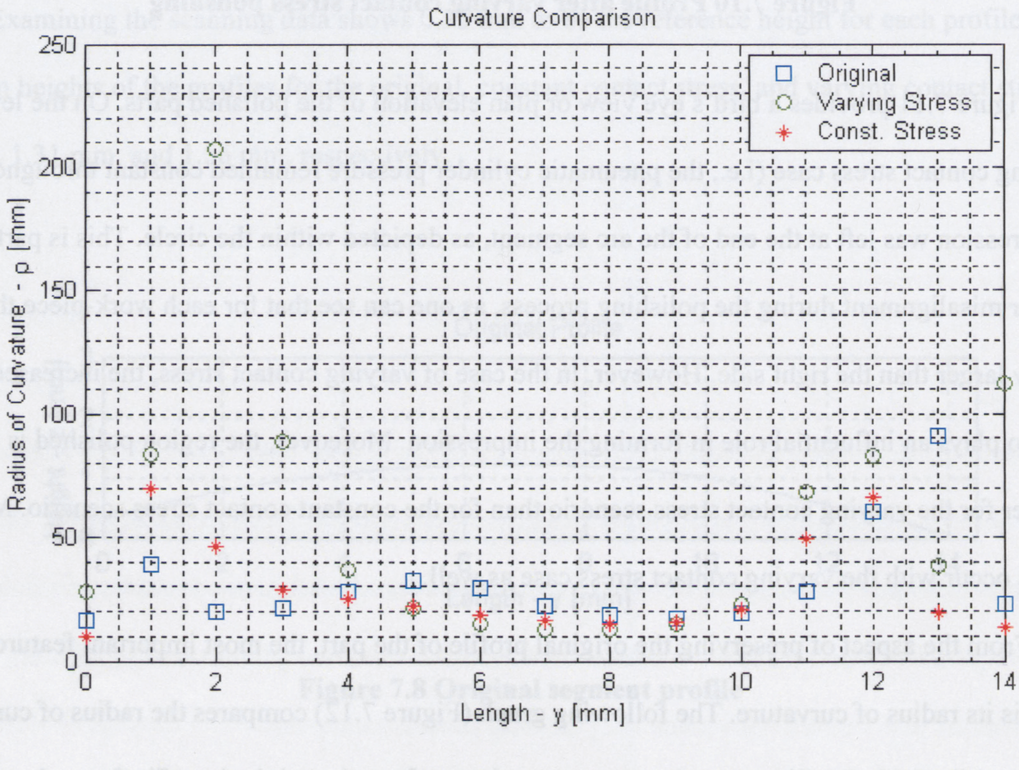

Figure 7.12 Comparison of the radii of curvature for each part

Table 7.1: Percentage change comparison

Distance along the Arc's chord – y [mm]	Percentage change of varying contact stress [%]	Percentage change of constant contact stress [%]
0.0	68.13	41.10
1.0	111.95	78.21
2.0	932.05	131.66
3.0	312.04	35.58
4.0	33.42	8.25
5.0	35.02	31.33
6.0	48.57	35.38
7.0	43.99	28.77
8.0	31.27	18.77
9.0	12.12	7.49
10.0	19.75	9.16
11.0	141.51	75.19
12.0	37.38	9.37
13.0	57.71	78.72
14.0	392.46	39.38

Note: during the experiment – in the case of the varying contact stress (i.e., the pneumatic cylinder pressure remained fixed at 2.25 bars) – when the polishing tool began to approach the end of the arc segment, the spindle pressure dropped by 10 psi (from 90 psi to 80 psi). It was adjusted manually back to 90 psi. This effectively demonstrates the influence of increased contact stress on the rotational speed of the spindle (polishing tool). However, in the instance of performing polishing under a constant contact stress condition (i.e., the pneumatic cylinder pressure was varied accordingly), no such drop in spindle pressure occurred. This also points to the benefits of force/cylinder pressure parameter planning.

7.4 Summary

Although with an open loop system, where there are no feedback control signals to regulate the spindle speed or control cylinder pressure, and the potential effectiveness is never realized, the results of the experiment support the contact model theory and the predicated benefits of employing the parameter planning method. The original profile of the work-piece was preserved when the Hertzian contact model theory was applied via the parameter planning methodology. (This is the case despite minor angular misalignment between the tool and the part's normal plane.) Conversely, with varying contact stress due to the cylinder pressure remaining constant, the spindle pressure dropped significantly during the process and had to be adjusted, more material was removed, and a dramatic change occurred in the radius of curvature from the original part, near the ends of the arc segment.

CHAPTER 8: Conclusions

8.1 Contribution

This thesis research introduces a novel approach to Automated Polishing – to maintain a constant surface contact stress and preserve the work-piece profile, while the surface geometry varies. A Hertzian contact stress model was derived enabling the numerical simulation of the contact stress, friction torque, and spindle speed during polishing. Path planning or G-code augmentation is performed based on an already existing G-code file provided by the client. From this point of view, the methodology developed facilitates a standalone device, independent of the type of machine or robot used.

This contribution may also be considered a requirement to successfully design an end-of-arm-tool, which would be used in the Automated Polishing of free-form surfaces. Here, the focus was given, not so much to mechanical design, but to first investigating the tool-to-workpiece interaction. This study of interaction gives insight into the problem before exploring several mechanical designs of the end-of-arm-tooling.

8.2 Discussion

With the development of a Hertzian contact stress model between the polishing tool and the part, the relationships between contact stress, geometry and applied polishing force are established. Numerical simulation elucidates this. When the surface contact stress is held constant (which is the major objective), the force is shown to be a function of the contact region's geometry – that is, the ratio, k, of semi-minor to semi-major ellipse axis. It is also evident that friction torque (and hence rotational speed) is a function of the applied force and the contact region's geometry. However, both these relationships are very complex, given their highly nonlinear nature.

Through the application of numerical simulation, force/pneumatic cylinder pressure parameter planning was determined and corresponded to each tool-path generated point, for the applied force/cylinder pressure must be adjusted to maintain a constant contact stress, as the surface geometry varies. This emphasizes not only the necessity of an active end-effector (as opposed to solely passive), but a programmable active end-effector. With a device such as this, it could be mounted on a variety of machines for polishing.

In all instances, the coefficient of kinetic friction was assumed as 0.2, and pertaining to the polishing tool head, material properties given in previous research were used [30]. The open loop test performed verified the effectiveness of the force/cylinder pressure parameter planning. With the parameter planning method applied, the original profile is for the most part preserved with slight changes to the radius of curvature. Along the end portions of the arc segment, it is significantly better than the applied non-Hertzian approach. With the non-Hertzian case, the surface contact stress increases when polishing the end portions of the arc segment.

8.3 Future Work

As mentioned previously, this thesis documents the initial investigation of designing an active end-effector or end-of-arm-tool, to be used in Automated Polishing. Specifically, it investigates what dynamic interaction the tool must confront. Therefore, it is both desired and necessary to carry out additional testing to further this work.

First, the implications from assuming the value of the coefficient of kinetic friction (between the tool and the work-piece surface), and the values of Young's Modulus and Poisson's ratio (for the tool head), may be explored. By adjusting these values, one can study their effect, if any. Secondly, the proposed dynamic model and control scheme must be verified. Several unknowns are in the dynamic model (discussed in chapter 6), and parameter estimation is a technique that may resolve this. After this, closed-loop testing may begin on parts similar to those used in the open loop experiments. Since the applied polishing torque was assumed to be approximately equal to the resultant torque, undoubtedly the control system must be tuned.

Finally, different part geometries and materials may be used in experiments as an ultimate verification of the effectiveness of the force/pressure parameter planning.

Appendix-A

This appendix provides the Matlab programs used to do the numerical simulation and parameter planning. It also includes graphs pertaining to the valve response testing; these graphs illustrate the step responses and cross-correlations.

A1. Matlab Programs

A1.1 Contact Model Application

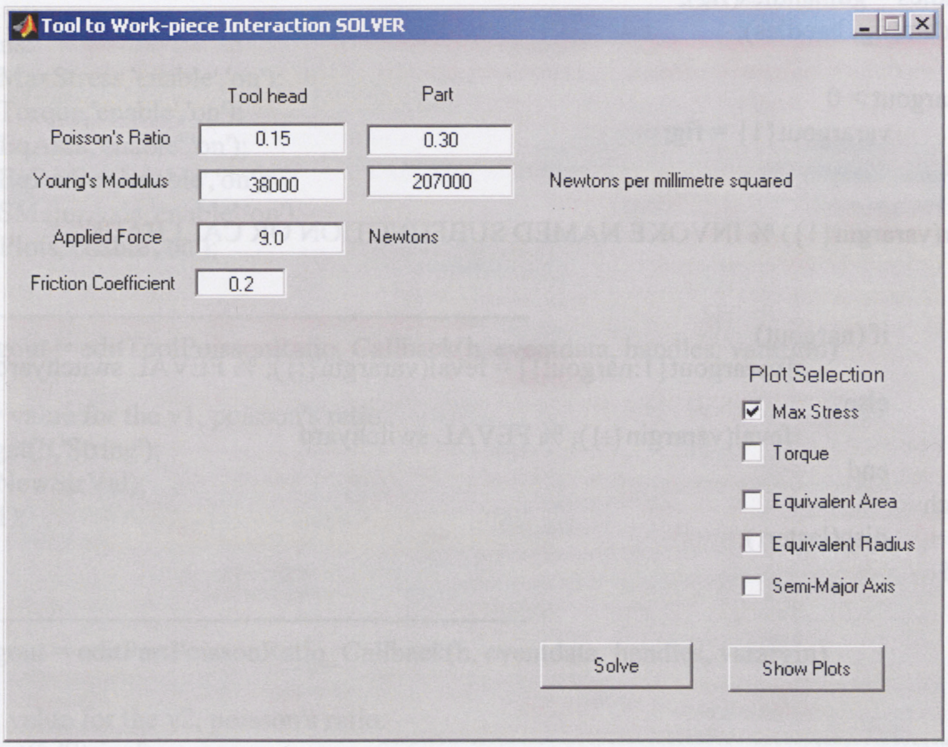

Figure A1. Graphic user interface for the contact stress model simulation

The above Figure illustrates the numeric simulation graphic user interface (GUI). Various parameters may be changed to match the particular materials used. In addition, the user has the option of select a specific plot.

The following is the main source code of the main program:

```
function varargout = TWI(varargin)
% TWI Application M-file for TWI.fig
%    FIG = TWI launch TWI GUI.
%    TWI('callback_name', ...) invoke the named callback.

% Last Modified by GUIDE v2.0 19-May-2004 15:37:37

if nargin == 0  % LAUNCH GUI

        fig = openfig(mfilename,'reuse');

        % Use system color scheme for figure:
        set(fig,'Color',get(0,'defaultUicontrolBackgroundColor'));

        % Generate a structure of handles to pass to callbacks, and store it.
        handles = guihandles(fig);
        guidata(fig, handles);

        if nargout > 0
                varargout{1} = fig;
        end

elseif ischar(varargin{1}) % INVOKE NAMED SUBFUNCTION OR CALLBACK

        try
                if (nargout)
                        [varargout{1:nargout}] = feval(varargin{:}); % FEVAL switchyard
                else
                        feval(varargin{:}); % FEVAL switchyard
                end
        catch
                disp(lasterr);
        end

end


% -----------------------------------------------------------------------
function varargout = pbSOLVE_Callback(h, eventdata, handles, varargin)

[BToA,k] = BToA_Data(0.01, 0.01, 0.99);

r2Prime= [200:100:1000]; %[1000:100:2000];     %radius in millimetres
r2 = [50:5:200]; %[200:100:1000];        %radius in millimetres

v1 = get(handles.editToolPoissonRatio,'Value');
v2 = get(handles.editPartPoissonRatio,'Value');
E1 = get(handles.editToolYoungsModulus,'Value');
E2 = get(handles.editPartYoungsModulus,'Value');
```

```
F = get(handles.editAppliedForce,'Value');
mu_k = get(handles.editMU_K,'Value');

[m,n1]=size(r2);
[m,n2]=size(r2Prime);
[m,n3]=size(F);
for j=1:n1 %corresponds to curvature r2
   for i=1:n2  %corresponds to r2Prime
      for o=1:n3
         [P_max(i,j,o),T(i,j,o),eA(i,j,o),eR(i,j,o), semiMajor(i,j,o)] = DataPoints2(BToA, k, r2(j),
r2Prime(i), v1, v2, E1, E2, F(o),mu_k);
      end
   end
end

c={P_max,T,eA,eR, semiMajor};
set(h,'UserData',c);

%enable buttons:
set(handles.cbMaxStress,'enable','on');
set(handles.cbTorque,'enable','on');
set(handles.cbEqArea,'enable','on');
set(handles.cbEqRadius,'enable','on');
set(handles.cbSMajorAxis,'enable','on');
set(handles.pbPlots,'enable','on');

% --------------------------------------------------------------------
function varargout = editToolPoissonRatio_Callback(h, eventdata, handles, varargin)

% Get the new value for the v1, poisson's ratio.
NewStrVal = get(h,'String');
v1 = str2num(NewStrVal);
set(h,'Value',v1);


% --------------------------------------------------------------------
function varargout = editPartPoissonRatio_Callback(h, eventdata, handles, varargin)

% Get the new value for the v2, poisson's ratio.
NewStrVal = get(h,'String');
v2 = str2num(NewStrVal);
set(h,'Value',v2);

% --------------------------------------------------------------------
function varargout = editToolYoungsModulus_Callback(h, eventdata, handles, varargin)

% Get the new value for the E1, young's modulus.
NewStrVal = get(h,'String');
E1 = str2num(NewStrVal);
set(h,'Value',E1);
```

```
% ------------------------------------------------------------------
function varargout = editPartYoungsModulus_Callback(h, eventdata, handles, varargin)

% Get the new value for the E2, young's modulus.
NewStrVal = get(h,'String');
E2 = str2num(NewStrVal);
set(h,'Value',E2);

% ------------------------------------------------------------------
function varargout = editAppliedForce_Callback(h, eventdata, handles, varargin)

% Get the new value for the F, applied force.
NewStrVal = get(h,'String');
F = str2num(NewStrVal);
set(h,'Value',F);



% ------------------------------------------------------------------
function varargout = pbPlots_Callback(h, eventdata, handles, varargin)

r2Prime= [200:100:1000]; %[1000:100:2000];     %radius in millimetres
r2 = [50:5:200]; %[200:100:1000];     %radius in millimetres
[R2,R2_PRIME]=meshgrid(r2,r2Prime);

UserData = get(handles.pbSOLVE,'UserData');

if get(handles.cbMaxStress,'value') == 1
   P_max = UserData{1};
   FigurePlot1 = figure('NumberTitle','off','Name','Relating Pressure to change in Curvature');
   handle1 = meshz(R2,R2_PRIME,P_max(:,:,1));
   %colormap(hot);
   %colorbar('vert');
   grid on; %grid minor;
   title('Maximum Stress vs Radii of Curvature');
   xlabel('R_2 [mm]'); ylabel('R"_2 [mm]'); zlabel('P_0 [N/mm^2]');
end

if get(handles.cbTorque,'value') == 1
   T = UserData{2};
   FigurePlot2 = figure('NumberTitle','off','Name','Relating Torque to change in Curvature');
   handle2 = meshz(R2,R2_PRIME,T(:,:,1));
   grid on; %grid minor;
   title('Elliptic Friction Torque vs Radii of Curvature');
   xlabel('R_2 [mm]'); ylabel('R"_2 [mm]'); zlabel('Torque [N.mm]');
end

if get(handles.cbEqArea,'value') == 1
   eA = UserData{3};
   FigurePlot3 = figure('NumberTitle','off','Name','Elliptic Area verses change in Curvature');
   handle3 = meshz(R2,R2_PRIME,eA(:,:,1));
```

```
    grid on; %grid minor;
    title('Elliptic Contact Area vs Radii of Curvature');
    xlabel('R_2 [mm]'); ylabel('R"_2 [mm]'); zlabel('Elliptic Area [mm^2]');
end

if get(handles.cbEqRadius,'value') == 1
    eR = UserData{4};
    FigurePlot4 = figure('NumberTitle','off','Name','Equivalent Contact Radius change in Curvature');
    handle4 = meshz(R2,R2_PRIME,eR(:,:,1));
    grid on; %grid minor;
    xlabel('R2 [mm]'); ylabel('R2 Prime [mm]'); zlabel('Equivalent Radius [mm]');
end

if get(handles.cbSMajorAxis,'value') == 1
    semiMajor = UserData{5};
    FigurePlot5 = figure('NumberTitle','off','Name','Semi-major axis (a) to change in Curvature');
    handle5 = meshz(R2,R2_PRIME,semiMajor(:,:,1));
    grid on; %grid minor;
    xlabel('R2 [mm]'); ylabel('R2 Prime [mm]'); zlabel('a [mm]');
end



% --------------------------------------------------------------------
function varargout = cbMaxStress_Callback(h, eventdata, handles, varargin)

% --------------------------------------------------------------------
function varargout = cbTorque_Callback(h, eventdata, handles, varargin)

% --------------------------------------------------------------------
function varargout = cbEqArea_Callback(h, eventdata, handles, varargin)

% --------------------------------------------------------------------
function varargout = cbEqRadius_Callback(h, eventdata, handles, varargin)

% --------------------------------------------------------------------
function varargout = cbSMajorAxis_Callback(h, eventdata, handles, varargin)

% --------------------------------------------------------------------
function varargout = editMU_K_Callback(h, eventdata, handles, varargin)
```

A1.2 Parameter planning source code

The following code pertains to augmenting the pressure G-code commands to the already existing path planning G-code.

```
function ParamPlan()
%read the path planning file and perform the pressure planning

print_to_file = 1;

[Ncodes,Gcodes,Xpts,Ypts,Zpts,Frate] = textread('averydata.txt','N%d G%d X%f Y%f Z%f F%f',-1);

flag = 0;
if flag == 1
FigurePlot1 = figure('NumberTitle','off','Name','Door Stop Profile');
handle1 = plot(Ypts,Zpts);
axis equal;
grid on; %grid minor;
title('Part Edge Profile');
xlabel('Part length - y [mm]'); ylabel('Part height - z [mm]');
end

%%%%%%%%%%%%%%%%%%%%%%%%%%%%%%%%%%%%%%%%%%%%%%%%%%%%%%%%%%
%%%%%%%%%%%%%%%%%%%%%%%%%%%%%%%%%%%%%%%%%%%%%%%%%%%%%%%%

px = polyfit(Ypts,Xpts,4);
px_prime = polyder(px);
px_doublePrime = polyder(px_prime);

Zx = polyval(px,Ypts);
Zx_prime = polyval(px_prime,Ypts);
Zx_doublePrime = polyval(px_doublePrime,Ypts);
Kxx = abs(Zx_doublePrime)./(1 + Zx_prime.^2).^1.5;
Rhox = 1./Kxx;
%plot(Ypts,Zpts,Ypts,Z);

TangentAngleXp = atan(Zx_prime)*180/pi;
BB = TangentAngleXp; %angle of normal; about the x-axis with REFERENCE TO THE Z-AXIS


py = polyfit(Ypts,Zpts,4);
py_prime = polyder(py);
py_doublePrime = polyder(py_prime);

Zy= polyval(py,Ypts);
Zy_prime = polyval(py_prime,Ypts);
Zy_doublePrime = polyval(py_doublePrime,Ypts);
Kyy = abs(Zy_doublePrime)./(1+Zy_prime.^2).^1.5;
Rhoy = 1./Kyy;
%plot(Ypts,Zpts,Ypts,Z);

TangentAngleYp = atan(Zy_prime)*180/pi;
AA = TangentAngleYp; %angle of normal; about the x-axis with REFERENCE TO THE Z-AXIS
```

```
%%%%%%%%%%%%%%%%%%%%%%%%%%%%%%%%%%%%%%%%%%%%%%%%%%%%%
%%%%%%%%%%%%%%%%%%%%%%%%%%%%%%
% CENTRAL DIFF METHOD
%%%%%%%%%%%%%%%%%%%%%%%%%%%%%%%%%%%%%%%%%%%%%%%%%%%%%
%%%%%%%%%%%%%%%%%%%%%%%%%%%%%%%

oY = size(Ypts);

[dx] = centraldiff(Xpts);
[dy] = centraldiff(Ypts);
[dz] = centraldiff(Zpts);

zPRIMEx = dz./dx;   %2 less than original
zPRIMEy = dz./dy;   %2 less than original
ozPrime = size(zPRIMEy);

[ddz] = centraldiff(zPRIMEy);

[row,col]=size(ddz);
b2=1;
for i=1:row
   b2 = b2+1;
   new_dy(i) = dy(b2);
   new_dx(i) = dx(b2);
   new_zPRIMEy(i) = zPRIMEy(b2);
   new_zPRIMEx(i) = zPRIMEx(b2);
end

zdPRIMEx = ddz./(new_dx');
zdPRIMEy = ddz./(new_dy');

Kx = abs(zdPRIMEx)./(1 + new_zPRIMEx'.^2).^1.5;
Ky = abs(zdPRIMEy)./(1 + new_zPRIMEy'.^2).^1.5;
rho_x = 1./Kx;
rho_y = 1./Ky;

TangentAngleY = atan(zPRIMEy')*180/pi;
TangentAngleX = atan(zPRIMEx')*180/pi;
A = 90 + TangentAngleY; %angle of normal; about the x-axis
B = 90 + TangentAngleX; %angle of normal; about the y-axis


%%%%%%%%%%%%%%%%%%%%%%%%%%%%%%%%%%%%%%%%%%%%%%%%%%%%%
%%%%%%%%%%%%%%%%%%%%%%%%%%%%%%
% FORWARD DIFF METHOD
%%%%%%%%%%%%%%%%%%%%%%%%%%%%%%%%%%%%%%%%%%%%%%%%%%%%%
%%%%%%%%%%%%%%%%%%%%%%%%%%%%%%%


[fdx] = forwardiff(Xpts);
[fdy] = forwardiff(Ypts);
```

```
[fdz] = forwardiff(Zpts);

zfPRIMEx = fdz./fdx;  %1 less than original
zfPRIMEy = fdz./fdy;  %1 less than original
ozfPrime = size(zfPRIMEy);

[fddz] = forwardiff(zfPRIMEy);

[row,col]=size(fddz);

for i=1:row
   new_fdy(i) = fdy(i);
   new_fdx(i) = fdx(i);
   new_zfPRIMEy(i) = zfPRIMEy(i);
   new_zfPRIMEx(i) = zfPRIMEx(i);
end

zdfPRIMEx = fddz./(new_fdx');
zdfPRIMEy = fddz./(new_fdy');

Kfx = abs(zdfPRIMEx)./(1 + new_zfPRIMEx'.^2).^1.5;
Kfy = abs(zdfPRIMEy)./(1 + new_zfPRIMEy'.^2).^1.5;
rho_fx = 1./Kfx;
rho_fy = 1./Kfy;

fTangentAngleY = atan(zfPRIMEy')*180/pi;
fTangentAngleX = atan(zfPRIMEx')*180/pi;
Af = 90 + fTangentAngleY; %angle of normal; about the x-axis
Bf = 90 + fTangentAngleX; %angle of normal; about the y-axis



%%%%%%%%%%%%%%%%%%%%%%%%%%%%%%%%%%%%%%%%%%%%%%%%%%%%%%%%%%%%%%%%%%%%%%%%%%%%%%%%%%%%%%%%%%%%%%%%%%%%%%%%%%%%%%%%%%%%%%%%%%%%%%%%%%%%%%%%%%%%%%%%%%%
% Calculating the Friction Torque and Force corresponding to the specified radius of curvature .........
%%%%%%%%%%%%%%%%%%%%%%%%%%%%%%%%%%%%%%%%%%%%%%%%%%%%%%%%%%%%%%%%%%%%%%%%%%%%%%%%%%%%%%%%%%%%%%%%%%%%%%%%%%%%%%%%%%%%%%%%%%%%%%%%%%%%%%%%%%%%%%%%%%%


[BToA,k] = BToA_Data(0.01, 0.01, 0.99);
v1 = 0.15; E1 = 38000;  %material properties for polishing head - Poisson's ratio & Young's modulus in
Newtons per millimetre squared
v2 = 0.30; E2 = 200000;
MaxPressure = 51; %units - N/mm^2

r1=inf;
r1Prime=inf;
r2= Rhoy';
r2Prime = 1000;    %radius in millimetres
phi = 0;
[m1,n]=size(k);
```

```
[m,n1]=size(r2);


for j=1:n1 %corresponds to curvature r2
   %for i=1:n2  %corresponds to r2Prime

% core of the function which is necessary to calculate kactual, the elliptic integral, and the delta value
....................

        if r1==inf & r1Prime == inf
          if r2(j) > r2Prime;
            rootA = 1./(2.*r2(j));
            rootB = 1./(2.*r2Prime);
            %fprintf(1,'\n\t***RADII OF CURVATURE WAS SWITCHED***\n\n');
         end
         if r2Prime > r2(j)
            rootA = 1./(2.*r2Prime);
            if r2(j) == 0
               rootB = inf;
            else
               rootB = 1./(2.*r2(j));
            end
            %fprintf(1,'\n\t***NORMAL OPERATION***\n\n');
         end
        else
         core = 0.25*(1/r1 + 1/r2(j) + 1/r1Prime + 1./r2Prime);
         plusOrMinusPart = 0.25*( ( (1/r1 - 1/r1Prime)+(1/r2(j) - 1./r2Prime) ).^2 - 4*(1/r1 -
1/r1Prime)*(1/r2(j) - 1./r2Prime)*sin(phi) ).^.5;
         rootA = (core - plusOrMinusPart)';
         rootB = (core + plusOrMinusPart)';
        end

        rootQuotient = rootB./rootA;
        if rootQuotient < 1 % invalid input value
          error('ERROR USING with rootQuotient function!');
        end

        %[m2,n] = size(rootQuotient)
        %for jj=1:m2
          for i=1:m1
            if (rootQuotient == BToA(i)) | (BToA(1) < rootQuotient)
               kActual=k(i);
               %fprintf(1,'\n\t***rootQuotient == BToA(i)) | (BToA(1) < rootQuotient***\n\n');
               break;
            end
            if (i<m1) & (BToA(i) > rootQuotient) & (BToA(i+1) < rootQuotient)
               slope =(BToA(i+1)-BToA(i))/(k(i+1)-k(i));
               kActual = ( (rootQuotient - BToA(i+1))/slope ) + k(i+1);
               break;
            end
            if  (BToA(m1) > rootQuotient)
```

```
            kActual=k(m1);
            break;
          end
        end
        %end

% calculation of properties ......

     kPrimeSquaredActual = 1-(kActual'.^2);
     [KActual,EActual]=ellipke(kPrimeSquaredActual);
     delta = (1./(rootA + rootB))*( (1-v1^2)/E1 + (1-v2^2)/E2 );
     mu_k = 0.2;    %coefficient of kinetic friction

% new stuff to calculate the new plots, etc ..........................................

     Peep_kActual(j) = kActual;
     Peep_Delta(j) = delta;
     Force(j) = 2*pi*(MaxPressure^3)*(EActual^2)*(delta^2)/(3*kActual);
     Torque(j) = (2/9)*mu_k*pi*(MaxPressure^4)*(EActual^3)*(delta^3)*(1+(1/kActual^3));

end

sz_A = size(A);
sz_F = size(Force);
sz_R = size(rho_y);
c2=1;
for i=1:sz_A(2)
  c2=c2+1;
  new_A(1)=A(1);
  new_A(oY(1)) = A(sz_A(2));
  new_A(c2) = A(i);

  new_B(1)=B(1);
  new_B(oY(1)) = B(sz_A(2));
  new_B(c2) = B(i);

  newForce(1)=Force(1);
  newForce(2)=Force(1);
  newForce(oY(1)-1) = Force(sz_F(2));
  newForce(oY(1)) = Force(sz_F(2));

  new_rho_y(1) = rho_y(1);
  new_rho_y(2) = rho_y(1);
  new_rho_y(oY(1)-1) = rho_y(sz_R(2));
  new_rho_y(oY(1)) = rho_y(sz_R(2));

  if i <= sz_F(2)
    newForce(c2+1) = Force(i);
  end
  if i <= sz_R(2)
    new_rho_y(c2+1) = rho_y(i);
```

```
  end
end

Ac = 3.0536e-5;
Pc = newForce'./(Ac*1e5);
Table = [Xpts Ypts Zpts new_A' new_B' newForce' Pc];  % Torque']

Xpts = 20.566 + Xpts; Ypts = 9.029+Ypts; Zpts = Zpts + 2.5; %this is for alignment with machine

Pconst = ones(oY(1),1)*2.5;
FrateForConstPress = ones(oY(1),1)*5;
Frate = ones(oY(1),1)*1;
PRINTFORMAT = [Ncodes Gcodes Xpts Ypts Zpts AA BB Pc Frate];
CONSTPRESS = [Ncodes Gcodes Xpts Ypts Zpts AA BB Pconst FrateForConstPress];

tag1 = size(PRINTFORMAT);
ii=1;
for i=1:tag1(1)
  if (PRINTFORMAT(i,1) >= 320 & PRINTFORMAT(i,1) <= 460)
    TRUNCFORMAT(ii,:) = PRINTFORMAT(i,:);
    TRUNCCONSTPRESS(ii,:) = CONSTPRESS(i,:);
    ii= ii+1;
  end
end

tag2 = size(TRUNCFORMAT);
index = tag2(1);
for i=1:tag2(1)
  ReverseRows1(index,:) = TRUNCFORMAT(i,:);
  ReverseRows2(index,:) = TRUNCCONSTPRESS(i,:);
  index=index-1;
end

COMBVARYING=[TRUNCFORMAT;ReverseRows1;TRUNCFORMAT;ReverseRows1]; %2 pass
varying pressure
COMBCONST=[TRUNCCONSTPRESS;ReverseRows2;TRUNCCONSTPRESS;ReverseRows2]; %2
pass CONSTANT pressure

tag3=size(COMBVARYING);
Nvalue=10;
for i=1:tag3(1)
  COMBVARYING(i,1) = Nvalue;
  COMBCONST(i,1) = Nvalue;
  Nvalue= Nvalue + 10;
end


fprintf(1,'\nN05    M03');
fprintf(1,'\nN%-6d G0%-6d X%-9.3f Y%-9.3f Z%-9.3f  A%-6.1f B%-6.1f P%-6.2f  F%-
6.1f\r',COMBVARYING');
fprintf(1,'N645    M05');
```

```
if print_to_file ==1
fid = fopen('newNCcode.nc','w');
fprintf(fid,'N05    M03\r');
fprintf(fid,'\nN%-6d G0%-6d X%-9.3f Y%-9.3f Z%-9.3f  A%-6.1f B%-6.1f P%-6.2f  F%-6.1f\r',COMBVARYING');
fprintf(fid,'\nN645    M05');
status = fclose(fid);


fid = fopen('CPNCcode.nc','w');
fprintf(fid,'N05    M03\r');
fprintf(fid,'\nN%-6d G0%-6d X%-9.3f Y%-9.3f Z%-9.3f  A%-6.1f B%-6.1f P%-6.2f  F%-6.1f\r',COMBCONST');
fprintf(fid,'\nN645    M05');
status = fclose(fid);
end
```

A2. Experimental Results

A2.1 Additional Valve Response Graphs

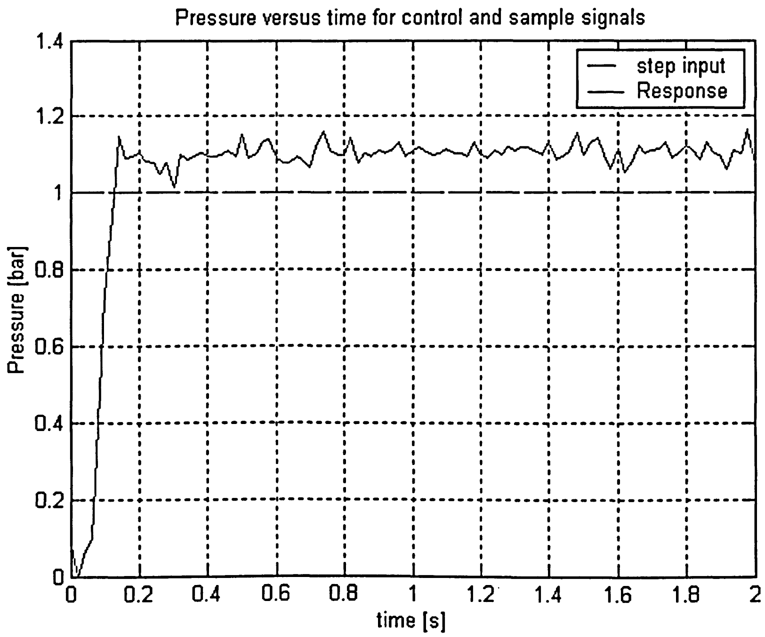

Figure A2. Step response for 1 bar

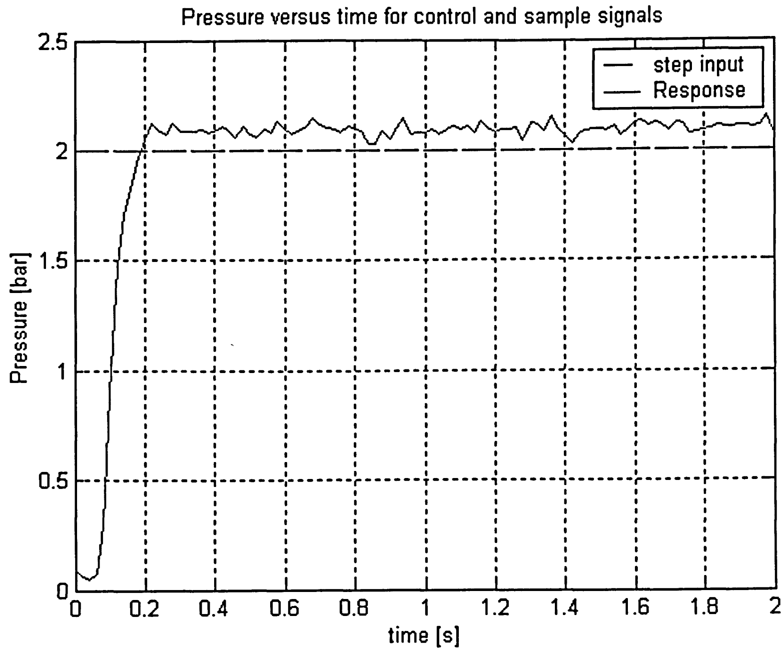

Figure A3. Step response for 2 bars

A2.2 Pressure Response and Cross-correlation Function Graphs

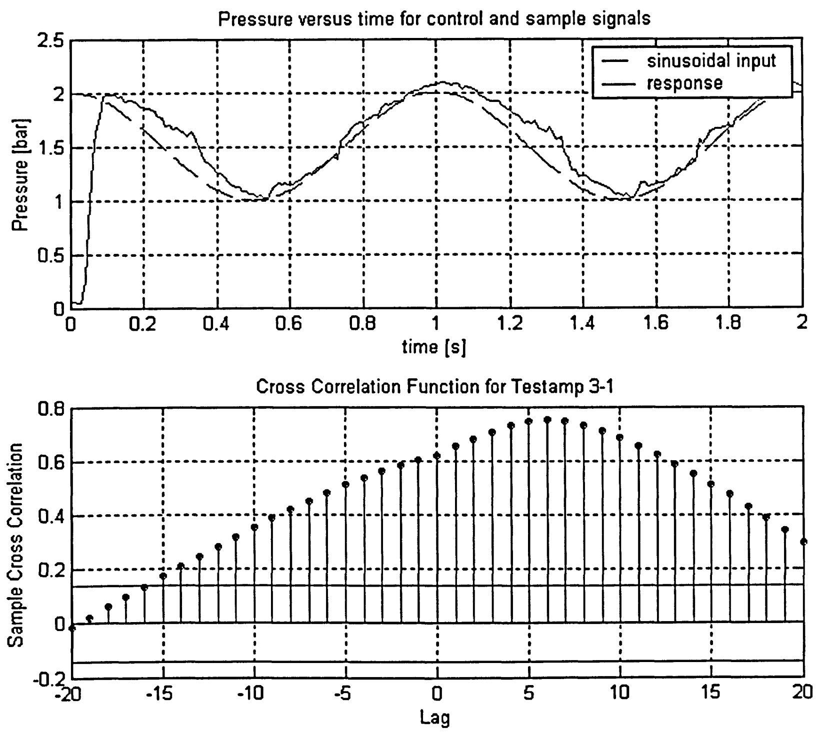

Figure A4. Testamp 3-1: Control frequency – 0.5 Hz, amplitude – 0.5 bars

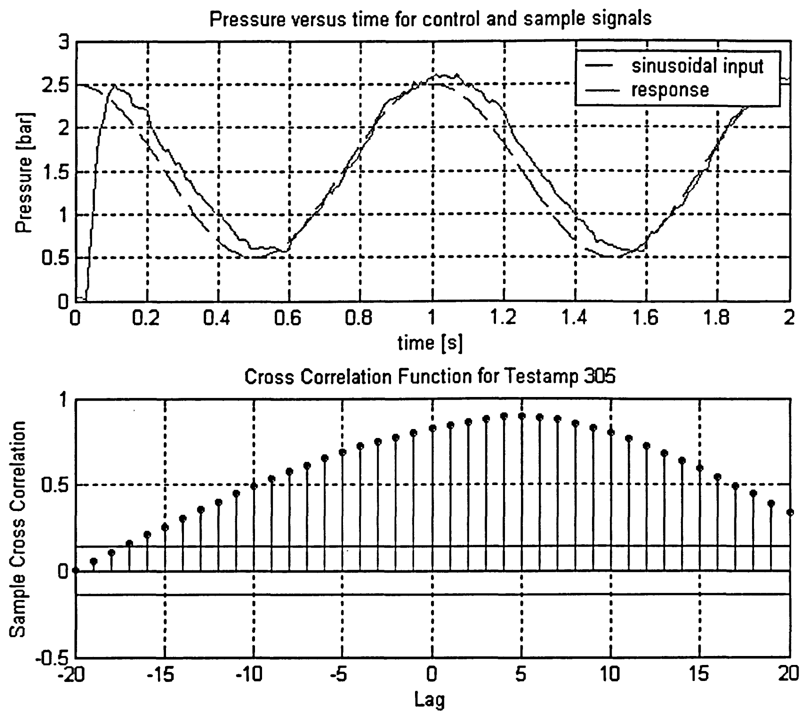

Figure A5. Testamp 305: Control frequency – 0.5 Hz, amplitude – 1 bar

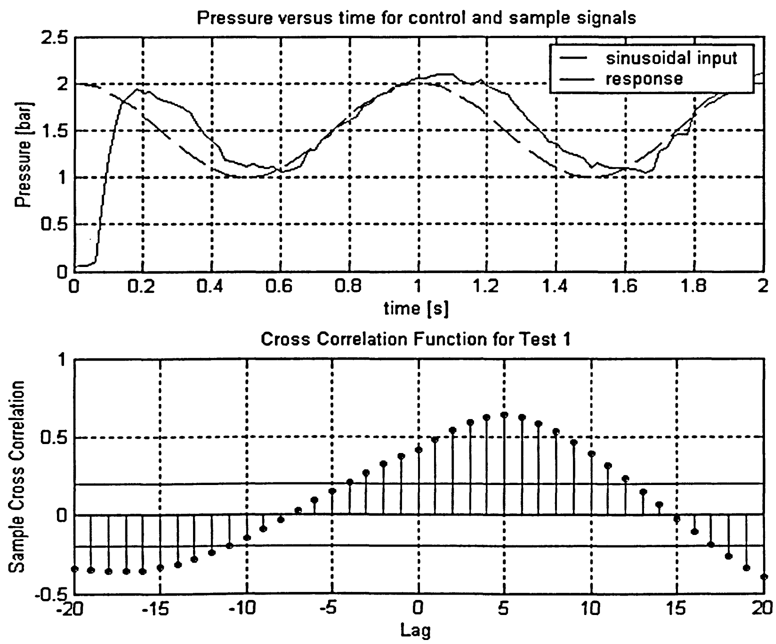

Figure A6. Test 1: Control frequency – 1 Hz, amplitude – 0.5 bars

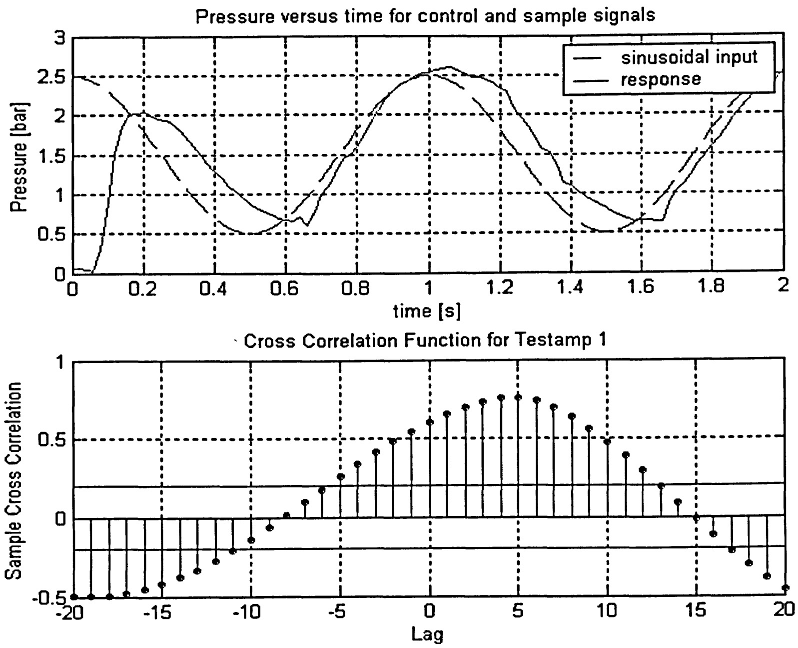

Figure A7. Testamp 1: Control frequency – 1 Hz, amplitude – 1 bars

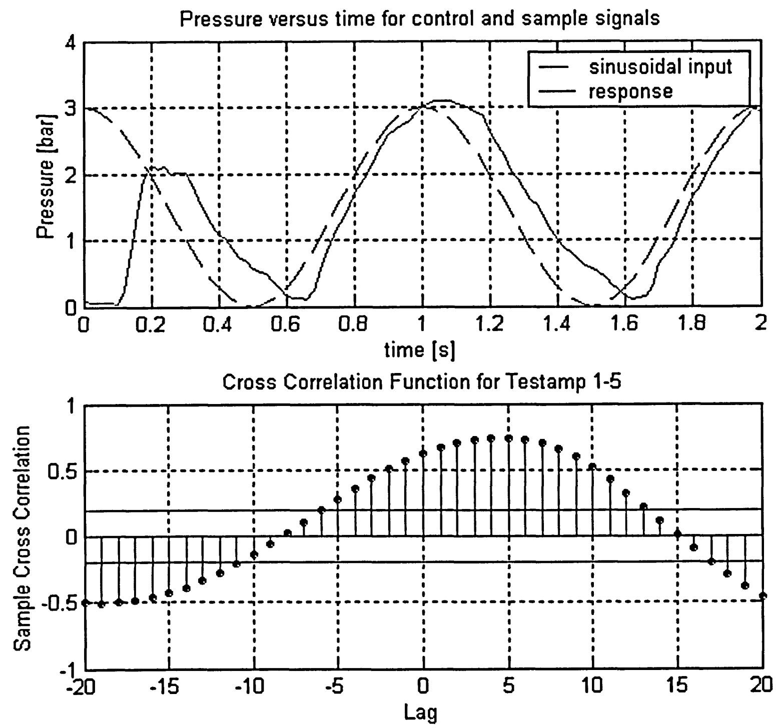

Figure A8. Testamp 1-5: Control frequency – 1 Hz, amplitude – 1.5 bars, mean – 1.5 bars

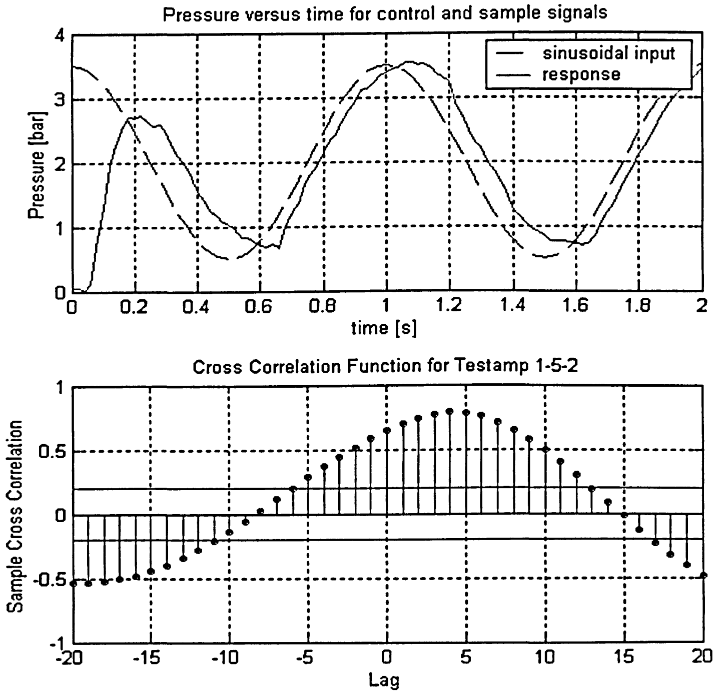

Figure A9. Testamp 1-5-2: Control frequency – 1 Hz, amplitude – 1.5 bars, mean – 2 bars

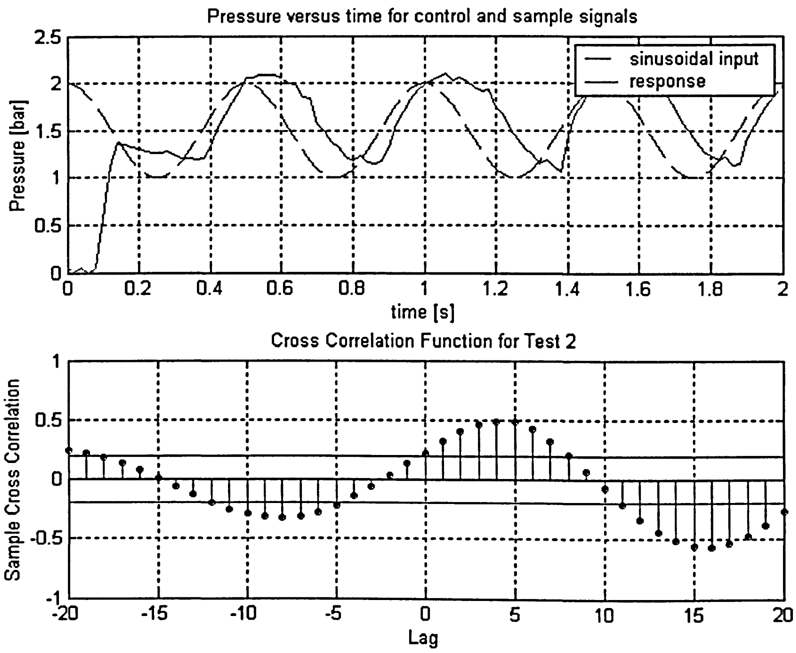

Figure A10. Test 2: Control frequency – 2 Hz, amplitude – 0.5 bars

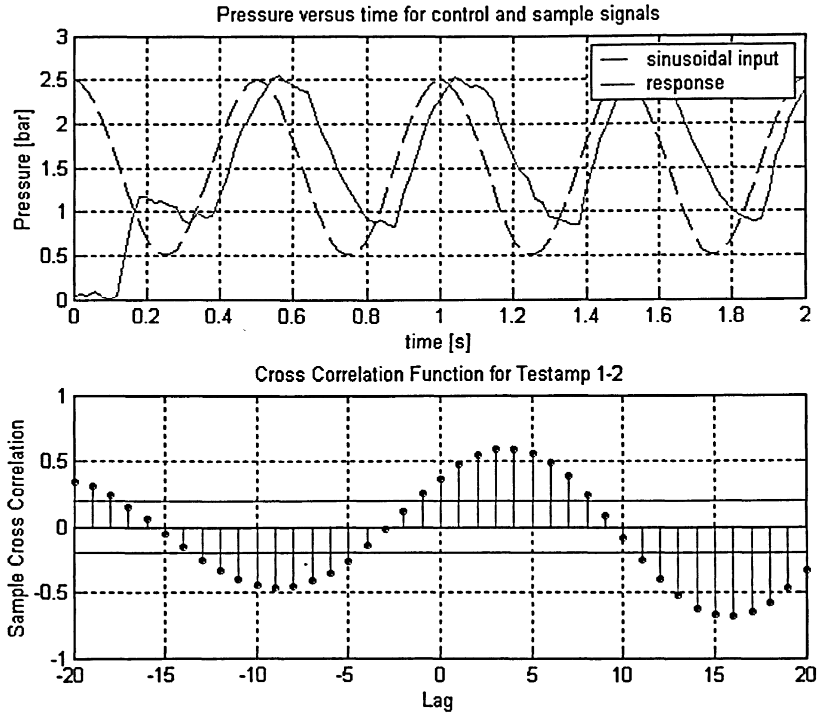

Figure A11. Testamp 1-2: Control frequency – 2 Hz, amplitude – 1 bars

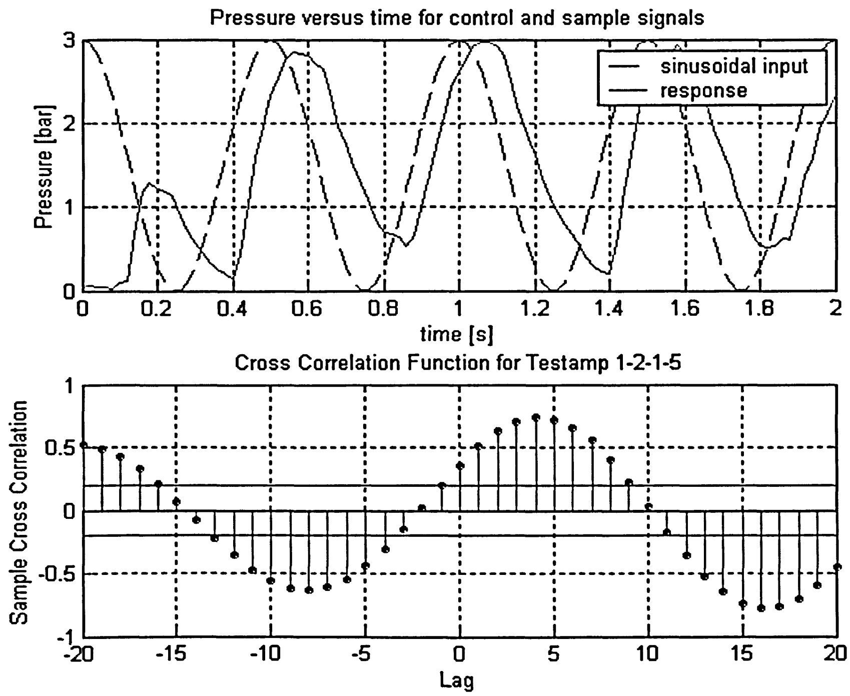

Figure A12. Testamp 1-2-1-5: Control frequency – 2 Hz, amplitude – 1.5 bars

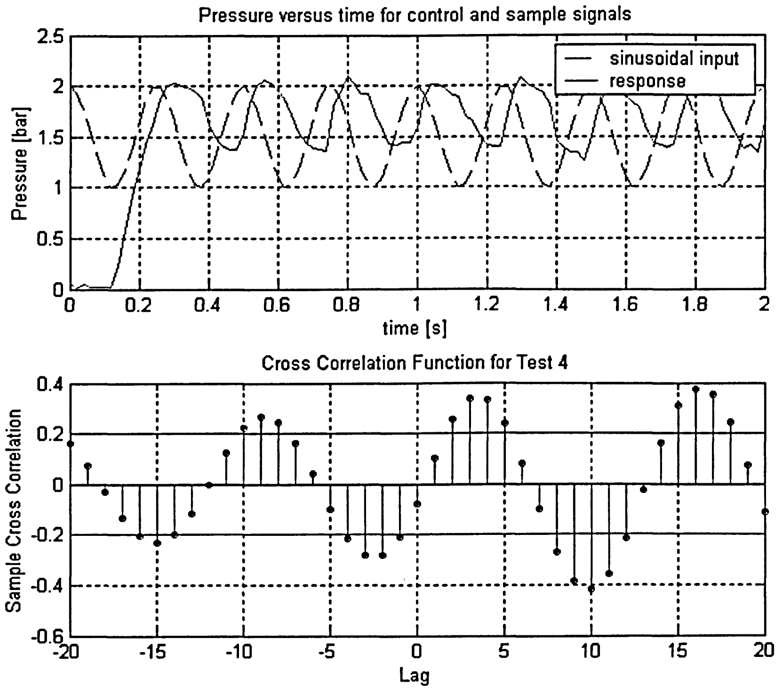

Figure A13. Test 4: Control frequency – 4 Hz, amplitude – 0.5 bars

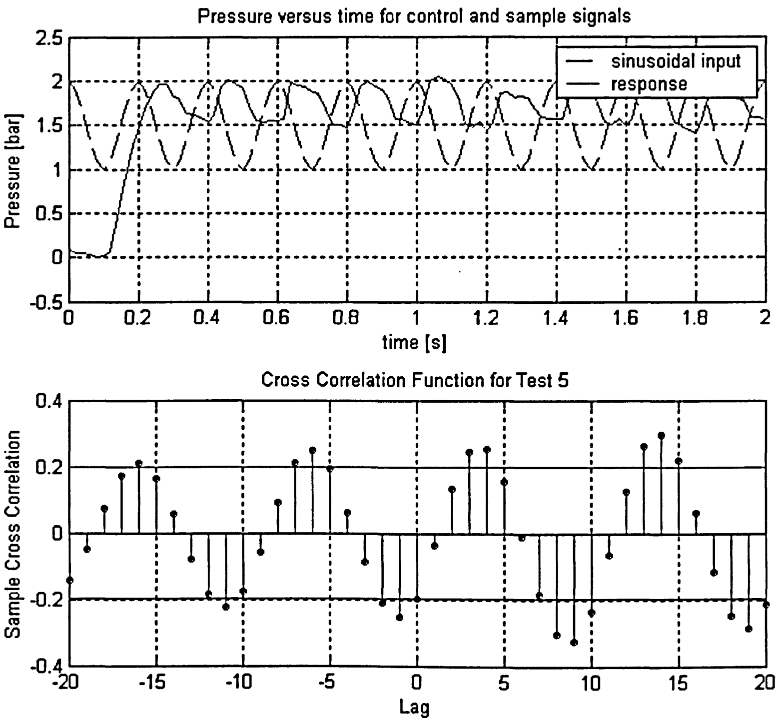

Figure A14. Test 5: Control frequency – 5 Hz, amplitude – 0.5 bars

References

1. Doyle, L. E., Keyser, C. A., Leach, J. L., Schrader, G. F., and Singer, M. B., *Manufacturing Processes and Materials for Engineers, 3rd Ed.,* 1985 (Prentice-Hall, Englewood Cliffs, New Jersey).

2. Guvenc, L. and Srinivasan, K., "An Overview of Robot-Assisted Die and Mold Polishing with Emphasis on Process Modeling," Journal of Manufacturing Systems (v16, n1, 1997), p49.

3. Huissoon, J. P., Ismail, F., Jafari, A., and Bedi, S., "Automated Polishing of Die Steel Surfaces," International Journal of Advanced Manufacturing Technology (200) 19:285-290.

4. Tam, H., Lui, O. C., Mok, and A. C.K., "Robotic polishing of free-form surfaces using scanning paths," Journal of Materials Processing Technology 95 (1999) 191-200.

5. Einav, O., "Large work envelope fully-automated aircraft panel polishing cell," Proceeding of the International Robotics & Vision Automation Conference: May 9-11, 1995, Detroit, Michigan

6. Sasaki, T., Miyoshi, T., and Saito, K., "Knowledge Acquisition and Automation of Polishing Operation for Injection Mold," Journal of the Japan Society of Precision Engineering, v 25, n 3, September, 1991.

7. Kawata, K., Sawada, Y., and Yamashita, M., "A New Method of Teaching and Path Generation for Automatic Die and Mold Polishing System," Japan/USA Symposium on Flexible Automation, v2 (ASME 1992)

8. Reed Business Information: ferret.com.au online publications by the global Reed Elsevier publishing group, http://www.ferret.com.au/articles/78/0c01a678.asp (June, 2004)

9. Manufacturingtalk published by Pro-Talk Ltd., based in the United Kingdom, http://www.manufacturingtalk.com/news/chb/chb107.html (June, 2004)

10. Product Finishing industry magazine, http://www.pfonline.com/articles/web050201.html (June, 2004)

11. Proctor, F. M., Murphy, K. N., "Advanced Deburring System Technology," ASME Winter Annual Meeting, PED 38, San Francisco, CA, (December 10 – 15, 1989). Published by ASME as PED-Vol. 38, Mechanics of Deburring and Surface Finishing Processes.

12. Engel T. W., Enomoto A., and Tomastik R. N., "Concept for Robotic Deburring Using Multipass Active Control," Journal of Vibration and Control, 3: 351-369, 1997.

13. Barratt A. J., Dissanayake M. W. M. G., Furukawa T., and Rye D. C., "Automated Polishing of an Unknown Three-dimensional Surface", Robotics & Computer Integrated Manufacturing (v12, n3, 1996), pp261-270.

14. Ahn J.H., Cha K.D., Go S. J., Jun C.S., Kim D.S., Lee M.C., and Lee M.H., "A robust trajectory tracking control of a polishing robot system based on CAM data," Robotics & Computer Integrated Manufacturing 17 (2003), pp177-183.

15. An, C. H., Hollerbach, J. M., "The Role of Dynamic Models in Cartesian Force Control of Manipulators," The International Journal of Robotics Research, Vol. 8, No. 4, August 1989.

16. Fisher, W. D., Mujtaba, M. S., "Hybrid Position/Force Control: A Correct Formulation," The International Journal of Robotics Research, Vol. 11, No. 4, August 1992.

17. Dawson, D. M., Dorsey, J. F., and Lewis, F. L., "Robust Force Control of a Robot Manipulator," The International Journal of Robotics Research, Vol. 11, No. 4, August 1992.

18. Bone, G. M., Elbestawi, M. A., "Active End Effector Control of a Low Precision Robot in Deburring," Robotics & Computer-Integrated Manufacturing, Vol. 8, No. 2, 1991.

19. Kazerooni, H., "Direct-Drive Active Compliant End Effector," IEEE Journal of Robotics and Automation, Vol. 4, No. 3, June 1988.

20. Ang (Jr.), M. H., Kah-Bin, L., and Tian-Soon, S., "A Compliant End-Effector Coupling For Vertical Assembly: Design And Evaluation," Robotics & Computer-Integrated Manufacturing, Vol. 13, No. 1, 1997.

21. Bausch, J. J., Kazerooni, H., and Kramer, B. M., "The Development of Compliant Tool Holders for Robotic Deburring,"

22. Xu, S. X., Zhan, J. M., Zhao, J., and Zhu, P. X., "Study of the Contact Force in Free-Form-Surfaces Compliant EDM polishing by Robot," Journal of Materials Processing Technology 129 (2002) 186-189.

23. Huang, H., Gong, Z. M., Chen, X. Q., and Zhou, L., "SMART Robotic System for 3D Profile Turbine Vane Airfoil Repair," International Journal of Advanced Manufacturing Technology (2003) 21:275-283.

24. Huang, H., Gong, Z. M., Chen, X. Q., and Zhou, L., "An Automated 3D Polishing Robotic System for Repairing Turbine Airfoil" The 3rd International Conference on Industrial Automation, Canada (June 1999, pp. 7-9).

25. Pusan National University, Measurement Control Lab, **http://mclab.me.pusan.ac.kr/index.htm**, (December 16, 2003).

26. PushCorp, Inc., Dallas, Texas, **http://www.pushcorp.com/**, (December 16, 2003).

27. Williams, J. A., Xie, Y., "The prediction of friction and wear when a soft surface slides against a harder rough surface," Wear 196 (1996) 21-34.

28. Kato K., "Abrasive wear of metals," Tribology International Vol. 30. No. 5, pp. 333-338, 1997.

29. Ahn J.H., Cho K.K., Jeong H.D., Kim S.R., and Lee, M.C., "Intelligently automated polishing for high quality surface formation of sculptured die," Journal of Materials Processing Technology 130-131 (2002) 339-344.

30. Zhang, L., Tam, H. Y., Yuan, C-M, Y-P Chen, Y-P, and Zhou, Z-D, "An investigation of material removal in polishing with fixed abrasives," Proceedings of the I MECH E Part B Journal of Engineering Manufacture (v216, 2002), p103-112.

31. Greenwood J.A., "Analysis of elliptic Hertzian contacts," Tribology International, Vol. 30, No. 3, pp. 235-237, 1997.

32. Chen T., Ye P., "A tool path generation strategy for sculptured surfaces machining," Journal of Materials Processing Technology 127 (2002) 369-373.

33. Chung Y. C., Park S. C., "Tool-path generation from measured data," Computer-Aided Design 35 (2003) 467-475

34. Dutta D., Sarma R., "Tool path generation for NC grinding," International Journal of Machine Tools Manufacture Vol. 38 No. 3, pp. 177-195, 1998.

35. Park S. C., "Tool-path generation for Z-constant contour machining," Computer-Aided Design 35 (2003) 27-36.

36. Ahamed S., van den Berg B., and Liang M., "A step based tool path generation system for rough machining of planar surfaces," Computer in Industry 32 (1996) 219-231.

37. Ghosh S. K., Lai T. Q., Li F., Wang X. C., and Wu T., "Tool-path generation for machining sculptured surface," Journal of Materials Processing Technology 48 (1995) 811-816.

38. Boresi, A. P., Schmidt, R. J., and Sidebottom, O. M., *Advanced Mechanics of Materials, 5th Ed.,* 1993 (John Wiley & Sons, Inc.)

39. Johnson, K. L., *Contact Mechanics*, 1985 (Cambridge University Press, Great Britain)

40. Xi F., Wanzhi H., Verner M., and Ross A., "Development of a sliding-leg tripod as an add-on device for manufacturing," Robotica (2001) v19, pp. 285-294.

41. Eastop, T. D., McConkey, A., *Applied Thermodynamics for Engineering Technologist, 5th Ed.,* 1993 (Longman Group UK Limited)

42. Slotine, J. E., Weiping, L., *Applied Nonlinear Control*, 1991 (Prentice Hall, New Jersey).